Dalton Transactions

PAPER

View Article Online
View Journal | View Issue

Cite this: *Dalton Trans.*, 2014, **43**, 14653

Iron(III) complexes of tripodal tetradentate 4N ligands as functional models for catechol dioxygenases: the electronic *vs.* steric effect on extradiol cleavage†

Mani Balamurugan,[a] Prabha Vadivelu[b] and Mallayan Palaniandavar *[a,c]

A few mononuclear iron(III) complexes of the type $[Fe(L)Cl_2]Cl$ **1–6**, where L is a tetradentate tripodal 4N ligand such as *N*,*N*-dimethyl-*N*′,*N*′-bis(pyrid-2-ylmethyl)ethane-1,2-diamine (**L1**), *N*,*N*-diethyl-*N*′,*N*′-bis-(pyrid-2-ylmethyl)ethane-1,2-diamine (**L2**), *N*,*N*-dimethyl-*N*′,*N*′-bis-(6-methylpyrid-2-ylmethyl)ethane-1,2-diamine (**L3**), *N*,*N*-dimethyl-*N*′-(pyrid-2-ylmethyl)-*N*′-(1-methyl-1*H*-imidazol-2-ylmethyl)ethane-1,2-diamine (**L4**), *N*,*N*-dimethyl-*N*′,*N*′-bis(1-methyl-1*H*-imidazol-2-ylmethyl)ethane-1,2-diamine (**L5**) and *N*,*N*-dimethyl-*N*′,*N*′-bis(quinolin-2-ylmethyl)ethane-1,2-diamine (**L6**), have been isolated and characterized by CHN analysis, UV-Visible spectroscopy and electrochemical methods. The complex cation $[Fe(H\mathbf{L1})Cl_3]^+$ **1a** possesses a distorted octahedral geometry in which iron is coordinated by the monoprotonated 4N ligand in a tridentate fashion and the remaining three sites of the octahedron are occupied by chloride ions. The DFT optimized octahedral geometries of **1**, **5** and **6** contain iron(III) with a high-spin (S = 5/2) ground state. The catecholate adducts $[Fe(L)(DBC)]^+$, where H_2DBC is 3,5-di-*tert*-butylcatechol, of all the complexes have been generated *in situ* in acetonitrile solution and their spectral and redox properties and dioxygenase activities have been studied. The DFT optimized geometries of the catecholate adducts $[Fe(\mathbf{L1})(DBC)]^+$, $[Fe(\mathbf{L5})(DBC)]^+$ and $[Fe(\mathbf{L6})(DBC)]^+$ have also been generated to illustrate the ability of the complexes to cleave H_2DBC in the presence of molecular oxygen to afford varying amounts of intra- (*I*) and extradiol (*E*) cleavage products. The extradiol to intradiol product selectivity (*E*/*I*, 0.1–2.0) depends upon the asymmetry in bidentate coordination of catecholate, as determined by the stereoelectronic properties of the ligand donor functionalities. While the higher *E*/*I* value obtained for $[Fe(\mathbf{L6})(DBC)]^+$ is on account of the steric hindrance of the quinolyl moiety to coordination the lower value observed for $[Fe(\mathbf{L4})(DBC)]^+$ and $[Fe(\mathbf{L6})(DBC)]^+$ is on account of the electron-releasing effect of the *N*-methylimidazolyl moiety. Based on the data obtained it is proposed that the detachment of the $-NMe_2$ group from the coordination sphere in the semiquinone intermediate is followed for dioxygen binding and activation to yield the extradiol cleavage product.

Received 6th August 2013,
Accepted 4th August 2014

DOI: 10.1039/c3dt52145a

www.rsc.org/dalton

Introduction

In nature, mononuclear non-heme iron enzymes perform a variety of important biological functions to maintain the carbon cycle. Biodegradation of naturally occurring aromatic molecules by soil bacteria involves the oxidative cleavage of catechol and other dihydroxy aromatics, which are the carbon sources for their growth.[1–5] Among them is the widely distributed mononuclear non-heme family of catechol dioxygenase enzymes, which particularly catalyze the oxidative cleavage[6] of catechol or its derivatives with insertion of both oxygen atoms of molecular oxygen into the aromatic ring of the substrate and convert the aromatic compounds into aliphatic compounds. Catechol dioxygenase enzymes can be classified into two types (Scheme 1), the intradiol-cleaving catechol dioxygenases, which use a non-heme iron(III) centre to catalyze the cleavage of the carbon–carbon bond between the two hydroxyl groups to give muconic anhydride, and the extradiol-cleaving catechol dioxygenases, which use a non-heme iron(II) centre to

[a]*School of Basic and Applied Sciences, Department of Chemistry, Central University of Tamil Nadu, Thiruvarur – 610 004, Tamil Nadu, India.*
E-mail: palanim51@yahoo.com, palaniandavarm@gmail.com, palaniandavar@cutn.ac.in
[b]*Chemical Sciences and Technology Division, National Institute for Interdisciplinary Science and Technology, CSIR, Trivandrum 695019, India*
[c]*School of Chemistry, Bharathidasan University, Tiruchirappalli – 620 024, Tamil Nadu, India*

†Electronic supplementary information (ESI) available. CCDC 949988. For ESI and crystallographic data in CIF or other electronic format see DOI: 10.1039/c3dt52145a

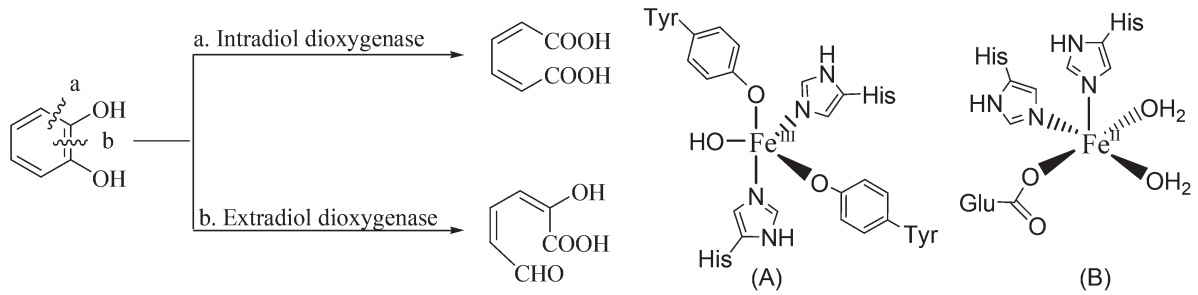

Scheme 1 Mode of cleavage of intradiol and extradiol dioxygenases: active site structures of intradiol- (A) and extradiol-cleaving (B) catechol dioxygenase enzymes.

catalyze the cleavage of the carbon–carbon bond adjacent to the two hydroxyl groups to yield 2-hydroxymuconic semialdehyde as the product.[7–12] The X-ray crystal structure of the intradiol-cleaving protocatechuate 3,4-dioxygenase (3,4-PCD) reveals that the enzyme possesses trigonal bipyramidal geometry in which the iron(III) centre is coordinated by four protein ligands (Tyr408, Tyr447, His460 and His462) and the fifth position is occupied by a solvent derived ligand.[8–10] Upon substrate (protocatechuic acid, H_2PCA) binding, the active site is converted into a square-pyramidal geometry and the axial Tyr447 and equatorial –OH are displaced by the substrate. In contrast to intradiol dioxygenases, extradiol dioxygenases contain an iron(II) centre and possess a 2-his-1-carboxylate facial triad structural motif ligated by two histidine and one glutamate amino acid residue and two water molecules in the active site forming a square pyramidal coordination geometry. In nature the biodegradation of aromatic molecules in the soil by extradiol cleavage exhibited by the extradiol-dioxygenase enzymes is the more common pathway and typically requires the iron(II) centre to utilize an oxygen activation mechanism.[8–17]

So, the development of synthetic model systems to investigate the mechanism of ring cleavage by extradiol-cleaving catechol dioxygenases has gained importance. Several iron(II/III) complexes have been successfully isolated as structural and functional models for both intradiol-[18–34] and extradiol-dioxygenases.[34–46] Earlier Que and co-workers synthesized several iron complexes of phenolate,[18] carboxylate[19] and nitrogen[20] donors as structural and functional models for these enzymes. Funabiki *et al.* also modeled the catechol dioxygenase enzymes using nitrogen and phenolate ligand donors.[21] Krüger[23] and Krebs[25] reported several iron(III) complexes of 4N ligands and observed the predominant formation of intradiol rather than extradiol cleavage products. Several other research groups also used different donor functionalities for making both the structural and functional mimics of catechol dioxygenases.[22,24,26–33] Palaniandavar *et al.* also successfully isolated several iron(III) complexes with pyridine/imidazole/benzimidazole and mono- and bis-phenolate ligand donor functionalities,[34] which are found to yield intradiol cleavage products exclusively or along with small amounts of extradiol cleavage products. Also, a few synthetic iron(III)-catecholate complexes of tridentate *cis*-facially coordinating 3N ligands like triazacyclononane (TACN)[35–38] and hydridotris(3,5-di-isopropyl-1-pyrazolyl)borate ($Tp^{i\text{-}pr^2}$)[39] have been studied as functional models for extradiol-cleaving catechol dioxygenase enzymes and up to 97% of extradiol cleavage product formation has been observed. Also, very recently, Gebbink *et al.* isolated iron(II)-catecholate complexes of 3,3-bis(1-alkylimidazol-2-yl) propionate-derived ligands[40] as structural and functional models for extradiol-dioxygenases. Palaniandavar *et al.* also successfully isolated iron(III) complexes of several linear 3N[44] and 3NO[45] ligands as functional models for the extradiol dioxygenases and correlated the dioxygenation reaction rate as well as extradiol cleavage yields with the ligand steric and electronic factors. Interestingly, many iron(III) complexes of facially coordinated tridentate 3N ligands elicit mostly extradiol-cleavage as they have a vacant/labile coordination site for dioxygen binding for extradiol cleavage to occur.[35–43]

Although several model complexes of 3N ligands have been reported to exhibit extradiol cleavage, functional models with 4N ligand donors exhibiting extradiol cleavage are very few in number as they have no vacant coordination site for dioxygen binding. Jang and coworkers reported the first iron(II) complex $[Fe(BLPA)(DBCH)]BPh_4$, where BLPA is bis(6-methyl-2-pyridylmethyl)(2-pyridylmethyl)amine and DBCH is 3,5-di-*tert*-butylcatecholate monoanion, which elicits 65% intradiol cleavage products along with 20% of extradiol products upon reaction with dioxygen.[22] The iron(III) complex $[Fe(L\text{-}N_4H_2)(DBC)]^+$, where L-N4H2 is 2,11-diaza[3,3](2,6)pyridinophane, affords both extra- and intradiol cleavage products.[27] Even though the adduct $[Fe(TPA)(DBC)]^+$, where TPA is the tripodal 4N ligand tris(pyrid-2-yl)methyl)amine, reacts with dioxygen to give 98% of the intradiol product,[20] a few iron(III) complexes of modified tetradentate 4N ligands such as $[Fe(6\text{-}Me_3TPA)(DBC)]^+$ and $[Fe(6\text{-}Me_2BPMCN)(DBC)]^+$ do not have a vacant coordination site for dioxygen binding, and also affords measurable amounts (3–12%) of extradiol cleavage products upon exposure to dioxygen.[43] Very recently, we have isolated the iron(III) complex $[Fe(L)Cl_2]^+$, where L is 1,4-bis(2-quinolylmethyl)-1,4-diazepane, which yields the highest amount of extradiol cleavage products (85%) in the presence of one equivalent of triethylamine and dioxygen.[46] However, the factors which determine the selectivity of the cleavage pathway for the complexes with 4N ligands are still unclear and need more studies. This prompted us to study the cleavage of catechols by iron(III) complexes of tripodal tetradentate 4N ligands (Scheme 2) as functional

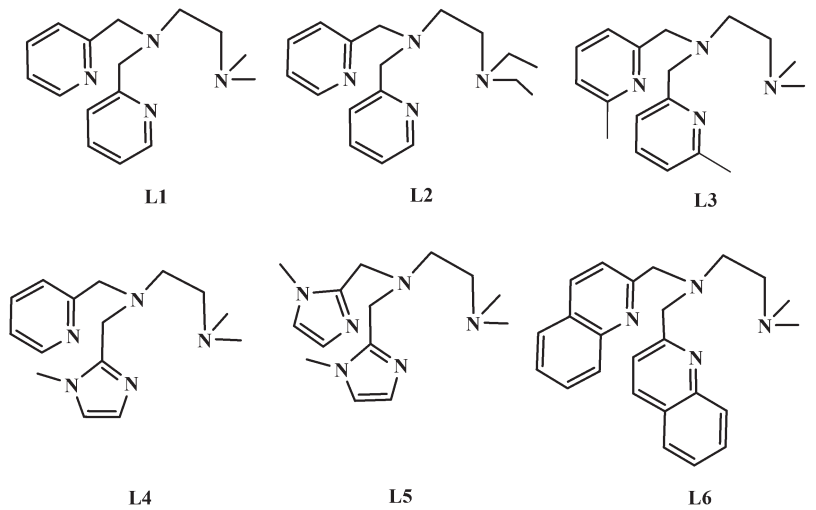

Scheme 2 Structures of 4N ligands used in the study.

models for catechol dioxygenase enzymes, with an aim to obtain extradiol cleavage exclusively and to collect evidence for the mechanistic pathway of the substrate-bound complex to facilitate dioxygen attack on the iron(III) centre to yield extradiol cleavage products. Also, we have already shown that incorporation of the sterically demanding $-NMe_2$ donor group in iron(III)-phenolate complexes[45] increases the Fe–O–C bond angle (133°, 148°) and hence the dioxygenase activity.

Experimental section

Materials

Pyridine-2-carboxaldehyde, *N*,*N*-dimethylethylenediamine, *N*,*N*-diethylethylenediamine, sodium triacetoxyborohydride, sodium borohydride, 1-methylimidazole-2-carboxaldehyde, 3,5-di-*tert*-butylcatechol (H_2DBC), 4-*tert*-butylcatechol (H_2TBC) (Aldrich), 6-methylpyridine-2-carboxaldehyde, quinoline-2-carboxaldehyde (Alfa Aesar), 3,4,5,6-tetrachlorocatechol (H_2TCC) (Lancaster), protocatechuic acid (3,4-dihydroxybenzoic acid, H_2PCA) (Loba, India) and iron(III) chloride (anhydrous) (Merck, India) were used as received. H_2DBC was recrystallized from hexane before use. The supporting electrolyte tetrabutylammonium perchlorate (Bu_4ClO_4, G. F. Smith, USA) was prepared using the procedure already reported[47] and recrystallized twice from aqueous ethanol. Methanol (Sisco Research Laboratory, Mumbai), acetonitrile, dichloromethane, diethylether and tetrahydrofuran (Merck, India) were distilled before use.

Syntheses of ligands

***N*,*N*-Dimethyl-*N*′,*N*′-bis(pyrid-2-ylmethyl)ethane-1,2-diamine (L1).** The ligand was prepared as reported[48] elsewhere. Yield: 1.19 g (88%). ^{1}H NMR (400 MHz, $CDCl_3$): δ 2.18 (s, 6H), 2.41 (t, 2H), 2.65 (t, 2H), 3.87 (s, 4H), 7.15 (t, 2H), 7.53 (d, 2H), 7.65 (t, 2H), 8.51 (d, 2H). EI-MS m/z = 270.1 $C_{16}H_{22}N_4^+$.

***N*,*N*-Diethyl-*N*′,*N*′-bis(pyrid-2-ylmethyl)ethane-1,2-diamine (L2).** The ligand was prepared as reported[49] elsewhere. Yield: 1.38 g (92%). ^{1}H NMR (400 MHz, $CDCl_3$): δ 1.12 (t, 6H), 2.28 (q, 4H), 2.49 (t, 2H), 2.58 (t, 2H), 3.83 (s, 4H), 7.18 (t, 2H), 7.49 (d, 2H), 7.68 (t, 2H), 8.61 (d, 2H). EI-MS m/z = 298.21 $C_{18}H_{26}N_4^+$.

***N*,*N*-Dimethyl-*N*′,*N*′-bis(6-methylpyrid-2-ylmethyl)ethane-1,2-diamine (L3).** The procedure employed for **L1** was used for the preparation of **L2**. 6-Methylpyridine-2-carboxaldehyde was used in place of pyridine-2-carboxaldehyde. The colourless oil formed was used without further purification for complex preparation. Yield: 1.25 g (84%). ^{1}H NMR (400 MHz, $CDCl_3$): δ 2.18 (s, 6H), 2.41 (t, 2H), 2.59 (s, 6H), 2.65 (t, 2H), 3.85 (s, 4H), 7.11 (d, 2H), 7.46 (d, 2H), 7.89 (t, 2H). EI-MS m/z = 298.2 $C_{18}H_{26}N_4^+$.

***N*,*N*-Dimethyl-*N*′-(1-methyl-1*H*-imidazol-2-ylmethyl)-*N*′-(pyrid-2-ylmethyl)ethane-1,2-diamine (L4).** The ligand was prepared as reported[49] elsewhere. Yield: 1.12 g (82%). ^{1}H NMR (400 MHz, $CDCl_3$): δ 2.13 (s, 6H), 2.44 (t, 2H), 2.63 (t, 2H), 3.67 (s, 3H), 3.58 (s, 2H), 3.78 (s, 2H), 6.78 (s, 1H), 6.86 (s, 1H), 7.17 (t, 1H), 7.46 (d, 1H), 7.63 (t, 1H), 8.58 (d, 1H). EI-MS m/z = 273.2 $C_{15}H_{23}N_5^+$.

***N*,*N*-Dimethyl-*N*′,*N*′-bis(1-methyl-1*H*-imidazol-2-ylmethyl)-ethane-1,2-diamine (L5).** The ligand was prepared as reported[49] elsewhere. Yield: 1.05 g (76%). ^{1}H NMR (400 MHz, $CDCl_3$): δ 2.14 (s, 6H), 2.41 (t, 2H), 2.59 (t, 2H), 3.68 (s, 6H), 3.59 (s, 4H), 6.80 (s, 2H), 6.87 (s, 2H). EI-MS m/z = 276.2 $C_{14}H_{24}N_6^+$.

***N*,*N*-Dimethyl-*N*′,*N*′-bis(quinolin-2-ylmethyl)ethane-1,2-diamine (L6).** The ligand was prepared as reported[49] elsewhere. Yield: 1.28 g (69%). ^{1}H NMR (400 MHz, $CDCl_3$): δ 2.13 (s, 6H), 2.42 (t, 2H), 2.62 (t, 2H), 3.80 (s, 4H), 7.15 (d, 2H), 7.42 (t, 2H), 7.57 (t, 2H), 7.67 (d, 2H), 7.89 (d, 2H), 8.13 (d, 2H). EI-MS m/z = 370.2 $C_{24}H_{26}N_4^+$.

Preparation of iron(III) complexes

[Fe(L1)Cl_2]Cl 1. A methanol solution (5 mL) of anhydrous $FeCl_3$ (0.162 g, 1 mmol) was added to a methanol solution (5 mL) of **L1** (0.27 g, 1 mmol) with stirring at room temperature for 30 min. The yellow complex (0.30 g, 82%) was filtered

off, washed with small amounts of cold methanol and diethylether and dried under vacuum. Yield, 0.33 g, 78%. ESI-MS m/z = 396 $[Fe(\mathbf{L1})Cl_2]^+$. Anal. Calcd $C_{16}H_{22}N_4Cl_3Fe$: C, 44.42; H, 5.13; N, 12.95. Found: C, 44.40; H, 5.14; N, 12.89.

$[Fe(HL1)Cl_2]Cl_2$ 1a. A methanol solution of one equiv. of HCl was added to the acetonitrile solution (5 mL) of **1** with stirring at room temperature and stirring was continued for 30 min. The slow evaporation of the methanol–acetonitrile solution of the complex gave yellow crystals, which are suitable for X-ray crystallographic analysis. Yield, 0.38 g, 82%. Anal. Calcd $C_{16}H_{23}N_4Cl_4Fe$: C, 40.97; H, 4.94; N, 11.95. Found: C, 40.93; H, 4.88; N, 11.92.

$[Fe(L2)Cl_2]Cl$ 2. The complex **2** was prepared using the procedure employed for isolating **1**. Yield, 0.33 g, 72%. ESI-MS m/z = 424 $[Fe(\mathbf{L2})Cl_2]^+$. Anal. Calcd $C_{18}H_{26}N_4Cl_3Fe$: C, 46.93; H, 5.69; N, 12.16. Found: C, 46.89; H, 5.68; N, 12.14.

$[Fe(L3)Cl_2]Cl$ 3. The complex **3** was prepared using the procedure employed for isolating **1**. Yield, 0.35 g, 76%. ESI-MS m/z = 424 $[Fe(\mathbf{L3})Cl_2]^+$. Anal. Calcd $C_{18}H_{26}N_4Cl_3Fe$: C, 46.93; H, 5.69; N, 12.16. Found: C, 46.92; H, 5.65; N, 12.13.

$[Fe(L4)Cl_2]Cl$ 4. The complex **4** was prepared using the procedure employed for isolating **1**. Yield, 0.30 g, 71%. ESI-MS m/z = 399 $[Fe(\mathbf{L4})Cl_2]^+$. Anal. Calcd $C_{15}H_{23}N_5Cl_3Fe$: C, 41.36; H, 5.32; N, 16.08. Found: C, 41.39; H, 5.37; N, 16.05.

$[Fe(L5)Cl_2]Cl$ 5. The complex **5** was prepared using the procedure employed for isolating **1**. Yield, 0.29 g, 67%. ESI-MS m/z = 402 $[Fe(\mathbf{L5})Cl_2]^+$. Anal. Calcd $C_{14}H_{24}N_6Cl_3Fe$: C, 38.34; H, 5.52; N, 19.16. Found: C, 38.33; H, 5.46; N, 19.11.

$[Fe(L6)Cl_2]Cl$ 6. The complex **6** was prepared using the procedure employed for isolating **1**. Yield, 0.37 g, 70%. ESI-MS m/z = 496 $[Fe(\mathbf{L6})Cl_2]^+$. Anal. Calcd $C_{24}H_{26}N_4Cl_3Fe$: C, 54.11; H, 4.92; N, 10.52. Found: C, 54.08; H, 4.86; N, 10.49.

Physical measurements

Elemental analyses were performed on a Perkin Elmer Series II CHNS/O Analyzer 2400. ^{1}H NMR spectra were recorded on a Bruker 400 MHz NMR spectrometer. The electronic spectra were recorded on an Agilent-8453 diode array spectrophotometer. Mass spectrometry was performed on a QTOF ESI-MS spectrometer. Cyclic voltammetry (CV) and differential pulse voltammetry (DPV) were performed using a three electrode cell configuration. A platinum sphere, a platinum plate and Ag(s)/Ag^+ were used as working, auxiliary and reference electrodes respectively. The supporting electrolyte used was Bu_4ClO_4 (TBAP). The temperature of the electrochemical cell was maintained at 25.0 ± 0.2 °C using a cryocirculator (HAAKE D8 G). By bubbling research grade nitrogen the solutions were deoxygenated and an atmosphere of nitrogen was maintained over the solutions during measurements. The $E_{1/2}$ values were observed under identical conditions for various scan rates. The instruments utilized included an EG & G PAR 273 Potentiostat/Galvanostat and a Pentium-IV computer along with the EG & G M270 software to carry out the experiments and to acquire the data. The product analysis was performed using a HP 6890 GC series Gas Chromatograph equipped with a FID detector and a HP-5 capillary column (30 m × 0.32 mm × 2.5 μm) and GC-MS analysis was performed on an Agilent GC-MS equipped with 7890A GC series (HP-5 capillary column) and 5975C inert MSD. The Density Functional Theory (DFT) calculations were performed with the g09 program[56] using the B3LYP basis function. While the metal center (Fe) was described by the LANL2DZ basis set along with the associated RECPs, the rest of the atoms were described by the 6-31G** basis set.

Crystallographic refinement and structure solution

The diffraction experiments were carried out on a Bruker SMART APEX diffractometer equipped with a CCD area detector. High quality crystals, suitable for X-ray diffraction, were chosen after careful examination under an optical microscope. Intensity data for the crystal was collected using MoK_α (λ = 0.71073 Å) radiation on a Bruker SMART APEX diffractometer equipped with a CCD area detector at 293 K. The SMART[50] program was used for collecting frames of data, indexing the reflections, and determining the lattice parameters; the SAINT[50] program was used for integration of the intensity of reflections and scaling. An empirical absorption correction was applied to the collected reflections with SADABS.[51] The structure was solved by direct methods using SHELXTL[52] and refined on F^2 by the full-matrix least-squares technique using the SHELXL-97[52] package. The structure was solved by the heavy atom method and other non-hydrogen atoms were located in successive difference Fourier syntheses. Crystal data and additional details of the data collection and refinement of the structure are presented in Table 1. The selected bond lengths and bond angles are listed in Table 2.

Reactivity studies

The catechol cleavage activity of all of the complexes toward H_2DBC was examined by exposing a solution of an iron(III)-DBC^{2-} adduct generated *in situ* in acetonitrile (ACN) to molecular oxygen. Kinetic analyses of the catechol cleavage reactions were carried out by time-dependent measurement of the disappearance of the lower-energy DBC^{2-}-to-iron(III) LMCT band. The solvents were equilibrated at the atmospheric pressure of O_2 at 25 °C and the solubility of O_2 in acetonitrile at 25 °C is 8.1×10^{-3} M.[53] A stock solution of the adducts $[Fe(L)(DBC)]^+$ was prepared by treating the complexes **1–6** (6×10^{-3} M) with an equivalent amount of H_2DBC pretreated with two equivalents of Et_3N. Oxygenation was started by rapid delivery of a stock solution (0.2 mL) of the catecholate adducts using a syringe to the O_2-saturated solvent (2.8 mL). The product analysis was carried out by adding the $[Fe(L)Cl_2]^+$ (0.1 mmol), H_2DBC (0.1 mmol) and triethylamine (0.2 mmol) to acetonitrile (15 mL) solvent under molecular oxygen and stirring for 24 h at room temperature. The oxygenation reaction was quenched by the addition of 6 M HCl (5 mL) and the products were extracted from the aqueous solution with diethylether (3 × 10 mL). The clear yellow organic layer was separated and dried over anhydrous Na_2SO_4 at room temperature. All the products were quantified using a GC (FID) with the following temperature program: injector temperature 130 °C; initial temperature 60 °C, heating rate 10 °C min^{-1} to

Table 1 Crystallographic data for **1a**

	1a
Empirical formula	$C_{16}H_{23}N_4Cl_4Fe$
Formula weight/g mol^{-1}	469.03
Crystal habit, colour	Yellow
Crystal system	Monoclinic
Crystal size	0.20 × 0.16 × 0.16 mm
Space group	*P*21/*c*
a/Å	12.9185(4)
b/Å	7.2101(2)
c/Å	23.6891(6)
α/°	90.000
β/°	102.369(2)
γ/°	90
V/Å^3	2155.27(10)
Z	4
ρ_{calcd}/g cm^{-3}	1.445
F(000)	964.0
T/K	293
No. of reflections collected	18 279
No. of unique reflections	5173
Radiation(MoKα)/Å	0.71073
Goodness-of-fit on F^2	1.040
Number of refined parameters	227
R_1/wR_2[$I > 2s(I)$][a]	0.0457/0.1099
R_1/wR_2 (all data)	0.0639/0.1198

[a] $R_1 = [\sum(||F_o| - |F_c||)/\sum|F_o|]$; w$R_2 = \{[\sum(w(F_o^2 - F_c^2)^2)/\sum(wF_o^4)]^{1/2}\}$.

Table 2 Selected bond lengths [Å] and bond angles [°] for **1a**

1a	
Bond lengths/Å	
Fe(1)–N(1)	2.177(3)
Fe(1)–N(2)	2.271(3)
Fe(1)–N(3)	2.200(7)
Fe(1)–Cl(1)	2.2769(11)
Fe(1)–Cl(2)	2.2822(12)
Fe(1)–Cl(3)	2.3010(11)
Bond angles/°	
N(1)–Fe(1)–N(3)	78.38(11)
N(1)–Fe(1)–N(2)	77.69(12)
N(3)–Fe(1)–N(2)	76.85(12)
N(1)–Fe(1)–Cl(1)	90.29(9)
N(3)–Fe(1)–Cl(1)	165.74(9)
N(2)–Fe(1)–Cl(1)	92.41(8)
N(1)–Fe(1)–Cl(2)	93.52(10)
N(3)–Fe(1)–Cl(2)	91.30(9)
N(2)–Fe(1)–Cl(2)	166.38(8)
Cl(1)–Fe(1)–Cl(2)	98.08(4)
N(1)–Fe(1)–Cl(3)	165.20(10)
N(3)–Fe(1)–Cl(3)	91.09(9)
N(2)–Fe(1)–Cl(3)	89.88(8)
Cl(1)–Fe(1)–Cl(3)	98.33(4)
Cl(2)–Fe(1)–Cl(3)	97.13(5)

130 °C, then increasing at a rate 2 °C min^{-1} to 160 °C and then increasing at a rate 5 °C min^{-1} to 260 °C; FID temperature 280 °C. The products were analyzed by GC three times and the average yields are listed in Table 2. GC-MS analysis was performed under conditions identical to those used for GC analysis and the oxygenation products were identified by comparing the observed retention times with those reported already.[41,44]

Results and discussion

Synthesis and characterization of ligands and iron(III) complexes

The tripodal tetradentate 4N ligands **L1–L6** (Scheme 2) were synthesized according to known procedures,[48,49] which involve Schiff base condensation and reductive amination. All the ligands, except for **L4**, were synthesized by reductive amination of *N*,*N*-dimethylethylenediamine or *N*,*N*-diethylethylenediamine with two moles of pyridine-2-carboxaldehyde (**L1**, **L2**) or 6-methyl- pyridine-2-carboxaldehyde (**L3**) or 1-methylimidazole-2-carboxaldehyde (**L5**) or quinoline-2-carboxaldehyde (**L6**) using sodium triacetoxyborohydride as a reducing agent and were characterized by ^{1}H NMR spectroscopy and mass spectrometry. The ligand **L4** was prepared by condensation of *N*,*N*-dimethylethylenediamine with pyridine-2-carboxaldehyde, followed by reduction of the resulting Schiff base, and reductive amination with 1-methylimidazole-2-carboxaldehyde. The iron(III) complexes [Fe(L)Cl$_2$]Cl **1–6** were isolated by treating anhydrous FeCl$_3$ with the corresponding ligands **L1–L6** in methanol with stirring. The complex **1a** was isolated by adding one equivalent of hydrochloric acid to an acetonitrile solution of **1**. All the complexes were characterized by elemental analysis and electronic spectroscopy and were formulated as [Fe(L)Cl$_2$]Cl based on elemental analysis. Conductivity measurements in acetonitrile solution (Λ_M, 80–125 Ω^{-1} cm^2 mol^{-1}) show that all the complexes behave as 1 : 1 electrolytes, and that both the chloride ligands remain coordinated. So, the octahedral complexes are formulated as [Fe(L)Cl$_2$]Cl. The X-ray crystal structure confirms the formulation of **1a** as [Fe(H**L1**)Cl$_3$]Cl. The tripodal ligands **L1–L6** with different donor functions are expected to display varying stereoelectronic effects and determine the pathway of catechol cleavage.

Description of the crystal structure of [Fe(HL1)Cl$_3$]Cl 1a

The molecular structure of the complex cation [Fe(H**L1**)Cl$_3$]$^+$ of **1a** is shown in Fig. 1 together with the atom numbering scheme and the selected bond lengths and bond angles are presented in Table 2. The complex cation possesses a distorted octahedral coordination geometry around iron(III) in which the two pyridyl nitrogen atoms (N1 and N3) and the central tertiary amine nitrogen atom (N2) of the tetradentate 4N ligand are facially coordinated to iron(III) and the remaining three coordination sites of the octahedron are occupied by chloride ions. The terminal tertiary amine nitrogen (N4) is protonated and so the tetradentate 4N ligand acts as a 3N donor. The Fe–N$_{py}$ (2.177(3), 2.200(7) Å) and Fe–N$_{amine}$ bond distances (2.271(3) Å) fall respectively in the ranges 2.143(4)–2.227(4) Å and 2.160(5)–2.334(7) Å observed for mononuclear iron(III) complexes reported in the literature.[34,44] The Fe–N$_{py}$ bonds are shorter than the Fe–N$_{amine}$ bond due to sp^2 and sp^3 hybridizations respectively of the pyridyl and tertiary amine nitrogen atoms.[25,44,54,55] Also, the lone-pair orbital on the central amine nitrogen atom is not oriented exactly toward the iron(III) orbital, rendering the Fe–N$_{amine}$ bond longer. Furthermore, all the Fe–Cl bonds (2.2769(11), 2.2822(12), 2.3010(11) Å) are

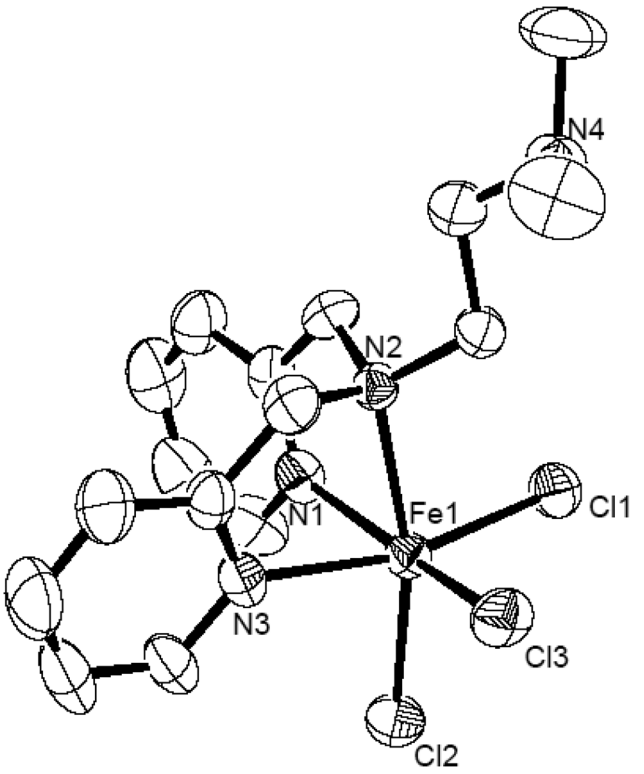

Fig. 1 Molecular structure of [Fe(HL1)Cl_3]Cl **1a** (50% probability factor for the thermal ellipsoid). Hydrogen atoms have been omitted for clarity.

longer than the Fe–N_{py} and Fe–N_{amine} bonds, as expected. The N–Fe–N, N–Fe–Cl and Cl–Fe–Cl (76.85(12)–98.33(4)°) and N–Fe–Cl (165.20(10)–166.38(8)°) bond angles deviate from the ideal octahedral angles of 90° and 180°, respectively, revealing the presence of significant distortion in the iron(III) coordination geometry.

Structures of 1, 5 and 6 and their DBC^{2-} adducts: density functional theory calculations

A DFT study was performed to investigate the geometries of **1**, **5** and **6** and their DBC^{2-} adducts. Initially, as a benchmark calculation, the crystal structure of **1a** was optimized and the computed geometry is in good agreement with the experimentally determined structure, except for slight elongations in bond lengths ranging from 0.02 to 0.21 Å (Fig. S1†). So, the same computational methodology was followed for optimizing the geometries of **1**, **5** and **6** and their DBC^{2-} adducts. Like **1a**, the complexes **1**, **5** and **6** also exhibit distorted octahedral coordination geometries (Fig. 2) containing iron(III) with high-spin (S = 5/2) rather than the low-spin (S = 1/2) ground state (Table 3). The optimized geometries of the catecholate adducts of these complexes, namely $[Fe(\mathbf{L1})(DBC)]^+$ (**1·DBC**$^{2-}$), $[Fe(\mathbf{L5})(DBC)]^+$ (**5·DBC**$^{2-}$) and $[Fe(\mathbf{L6})(DBC)]^+$ (**6·DBC**$^{2-}$), with high-spin state (S = 5/2) are provided also in Fig. 2.

The complex $[Fe(\mathbf{L1})Cl_2]^+$ **1** possesses a distorted octahedral geometry and the Fe–N_{py} bond (Fe–N1, 2.18 Å) is shorter than the Fe–N_{amine} bond (Fe–N2, 2.31; Fe–N4, 2.27 Å) due to sp^2 and sp^3 hybridizations respectively of the pyridyl and tertiary amine nitrogen atoms. However, the other Fe–N_{py} bond (Fe–N3, 2.28 Å) is longer than the Fe–N_{amine} bond (Fe–N4, 2.27 Å) due to the *trans* effect exerted by the chloride ion *trans* to the pyridyl N3 nitrogen. The optimized structure of $[Fe(\mathbf{L5})Cl_2]^+$ **5** is similar to that of **1** and the Fe–N4 (**1**, 2.27; **5**, 2.28 Å), Fe–Cl1 (**1**, 2.32; **5**, 2.33 Å) and Fe–Cl2 (**1**, 2.26; **5**, 2.25 Å) bond lengths are nearly equal to the respective bonds in **1**. The Fe–N_{im} bond in **5** (Fe–N3, 2.17 Å) is shorter than the Fe–N_{py} bond in **1** (Fe–N3, 2.28 Å) revealing that the imdazolyl nitrogen in **5** is coordinated more strongly than the pyridyl nitrogen in **1** (pK_a, BH^+: ImH^+, 7.2; pyH^+, 5.6) and concomitantly, the Fe–N_{amine} (Fe–N2, 2.43 Å) and Fe–N1 (**1**, 2.18; **5**, 2.16 Å) bonds are weaker than those in **1** (Fe–N2, 2.31 Å). The stronger coordination of the imidazolyl ligand in **5** is expected to stabilize its HOMO, which is reflected in the larger SOMO–LUMO gap in **5** (0.23 a.u) than that in **1** (0.20 a.u). The optimized structure of $[Fe(\mathbf{L6})Cl_2]^+$ **6** is also similar to that of **1** and the Fe–$N4_{amine}$ (2.28 Å), Fe–Cl1 (2.34 Å) and Fe–Cl2 (2.25 Å) bond lengths are nearly equal to those in **1**. The Fe–$N3_{amine}$ bond in **6** (Fe–N3, 2.26 Å) is shorter than the Fe–$N3_{amine}$ bond in **1** due to weaker coordination of one of the quinolyl nitrogen donors (Fe–N2, 2.53 Å), revealing that the steric effect of the quinolyl donor is more important than its electronic effect.

The optimized geometry of **1** is helpful in discussing the effect of protonation of complex **1**. Upon protonation of the –NMe_2 donor in **1**, the Fe–NMe_2 coordinate bond is broken and concomitantly the Fe–N_{amine} (**1**, 2.31; **1a**, 2.27 Å) and Fe–Cl1 (**1**, 2.32; **1a**, 2.27 Å) bonds become stronger and the Fe–N3 bond (**1**, 2.28; **1a**, 2.20 Å) becomes weaker with the Fe–N_{py} bond strength (Fe–N1, **1**, 2.18; **1a**, 2.17 Å) remaining constant.

Upon displacing the chloride ions in **1** by bidentate DBC^{2-} dianions to obtain the adduct $[Fe(\mathbf{L1})(DBC)]^+$ (Fe–O1, 2.08; Fe–O2, 2.01 Å), both the Fe–$N1_{py}$ (2.27 Å) and Fe–$N4_{amine}$ (2.35 Å) bonds are weakened while the Fe–$N2_{py}$ (2.20 Å) and Fe–$N3_{amine}$ bonds (2.30 Å) are strengthened. Similarly, upon displacing the chloride ions in **5** by DBC^{2-} to form $[Fe(\mathbf{L5})(DBC)]^+$, the Fe–$N4_{amine}$ (2.37 Å) bond is weakened while the Fe–$N3_{amine}$ (2.38 Å) bond is strengthened. As in **5**, the Fe–$N2_{im}$ bond (2.16 Å) in the adduct is stronger than the corresponding Fe–$N2_{py}$ bond in $[Fe(\mathbf{L1})(DBC)]^+$; however, the Fe–$N1_{im}$ (2.27 Å) bond is equal to that of the Fe–$N1_{py}$ (2.27 Å) bond. Also, as in **5** and **1**, the spin density of the iron(III) center in **5·DBC**$^{2-}$ (ρ, 3.77) is higher than that in **1·DBC**$^{2-}$ (ρ, 3.75) and the SOMO–LUMO gap is larger in **5·DBC**$^{2-}$ (0.15 a.u) than that in **1·DBC**$^{2-}$ (0.12 a.u). Upon displacing the chloride ions in **6** by DBC^{2-} to give **6·DBC**$^{2-}$, the Fe–$N4_{amine}$ (2.37 Å) bond becomes weaker, as for **1·DBC**$^{2-}$ and **5·DBC**$^{2-}$. Interestingly, the weakly coordinated quinolyl moiety in **6** becomes coordinated more strongly (Fe–$N2_{quin}$, 2.26 Å) and the other quinolyl nitrogen becomes weakly bound (Fe–$N2_{quin}$, 2.33 Å). Also, the Fe–N_{quin} bonds are weaker than the corresponding Fe–N_{py} bonds in **1·DBC**$^{2-}$, as expected (*cf.* above). Thus for **1**, **5** and **6** the Fe–NMe_2 bond is elongated upon adduct formation with DBC^{2-}. Also, a remarkable variation in asymmetry of the coordinate bonds of DBC^{2-} (**1**, Fe–O1, 2.08; Fe–O2, 2.01: **5**, Fe–O1,

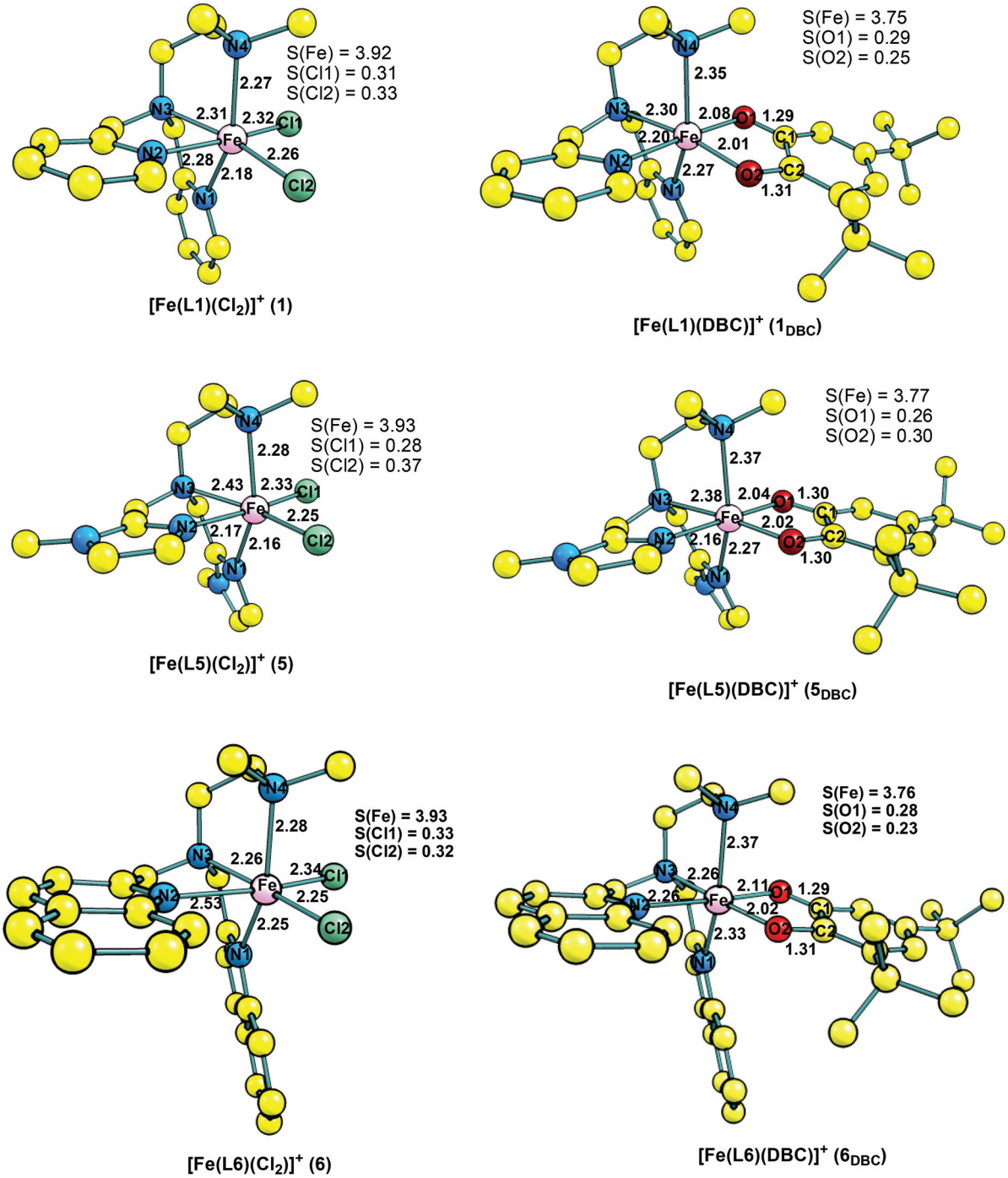

Fig. 2 The optimized geometries of $[Fe(\mathbf{L1})Cl_2]^+$ (**1**), $[Fe(\mathbf{L5})Cl_2]^+$ (**5**) and $[Fe(\mathbf{L6})Cl_2]^+$ (**6**) and their catecholate derivatives $[Fe(\mathbf{L1})(DBC)]^+$ (**1**·DBC^{2-}), $[Fe(\mathbf{L5})(DBC)]^+$ (**5**·DBC^{2-}) and $[Fe(\mathbf{L6})(DBC)]^+$ (**6**·DBC^{2-}) in their S = 5/2 spin state. Selected bond lengths (Å) along with the key spin densities are given.

2.04; Fe–O2, 2.02: **6**, Fe–O1, 2.02; Fe–O2, 2.01 Å), as dictated by the stereoelectronic factors of ligand donor functionalities, has been observed (*cf.* below).

Electronic absorption spectral studies

The electronic absorption spectra of $[Fe(L)Cl_2]Cl$ **1–6** in acetonitrile solution exhibit a band in the range 350–370 nm (Table 4), which is assigned to the $Cl^- \rightarrow Fe(III)$ ligand to metal charge transfer (LMCT) transition.[25] The more intense band in the range 240–250 nm is caused by $\pi \rightarrow \pi^*$ transitions within the ligands. When H_2DBC pretreated with two equivalents of Et_3N is added to **1–6** in acetonitrile, two catecholate-to-iron(III) LMCT bands appear in the ranges 500–570 and 850–920 nm (Fig. 3, Table 4), which are assignable to DBC^{2-}-to-Fe(III) LMCT

Table 3 Relative stability of [Fe(**L1**/**L5**)(Cl_2)]$^+$ and [Fe(**L1**/**L5**)(DBC)]$^+$ complexes in their high-spin (S = 5/2) and low-spin (S = 1/2) states. Free energies in kJ mol^{-1}

	Relative stability in kJ mol^{-1}	
Complexes	High spin (S = 5/2)	Low spin (S = 1/2)
[Fe(**L1**)(Cl_2)]$^+$	0.0	+53.2
[Fe(**L1**)(DBC)]$^+$	0.0	+42.3
[Fe(**L5**)(Cl_2)]$^+$	0.0	+64.8
[Fe(**L5**)(DBC)]$^+$	0.0	+58.0

transitions[22–34,44–46] involving two different catecholate orbitals on the chelated DBC^{2-}. When one mole of Et_3N is added to the catecholate adducts no change in absorptivity of the bands is observed, suggesting that H_2DBC is completely deprotonated and is coordinated to iron(III) bound to all the four nitrogen atoms of the tetradentate ligand (Scheme 3).[20,25–27,46]

The energies of both the DBC^{2-}-to-Fe(III) LMCT bands of the adducts [Fe(L)(DBC)]$^+$ show a remarkable dependence on the ligand donors of the primary ligands: **L1** > **L2** > **L3** < **L4** < **L5** > **L6**.[20–34,43–46] Similar trends in band energies are observed for the high energy band of all the adducts of other catechols. Upon replacing the $-NMe_2$ group in [Fe(**L1**)(DBC)]$^+$ by the $-NEt_2$ group to obtain [Fe(**L2**)(DBC)]$^+$ both the LMCT bands are shifted to lower energies. The weaker coordination of the sterically hindering $-NEt_2$ group causes a decrease in the negative charge on the iron(III) centre, which stabilizes the dπ* orbitals of iron(III) leading to a decrease in energy gap[18] between the dπ* orbital and the ligand catecholate orbitals, and hence the observed decrease in the catecholate-to-iron(III) LMCT band energy. Similarly, upon replacing both the pyridyl arms in [Fe(**L1**)(DBC)]$^+$ by 6-methylpyridyl arms to obtain [Fe(**L3**)(DBC)]$^+$ the LMCT bands are shifted to lower energies. The steric bulk of the 6-Me group renders the lone pair orbital on pyridyl nitrogen not oriented exactly towards the iron(III) orbital and causes the negative charge built on the iron(III) centre to decrease. Upon replacing one and two of the pyridyl arms in [Fe(**L1**)(DBC)]$^+$ by one and two of the imidazolyl arms to get respectively [Fe(**L4**)(DBC)]$^+$ and [Fe(**L5**)(DBC)]$^+$ the LMCT bands are shifted to higher energies in both the adducts. The stronger coordination of the imidazolyl group (*cf.* above) raises the energy of the iron(III) dπ* orbital, leading to higher LMCT band energies. However, upon replacing the pyridylmethyl arms in [Fe(**L1**)(DBC)]$^+$ by the sterically hindering quinolylmethyl arms the LMCT bands are shifted to lower energies as observed for [Fe(**L3**)(DBC)]$^+$ with sterically hindering 6-methylpyridyl arms (*cf.* above). Thus the Lewis acidity of the iron(III)

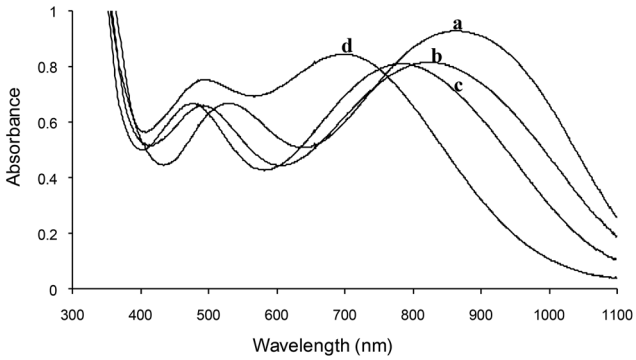

Fig. 3 Electronic absorption spectra of adducts of **2** (2×10^{-4} M) generated *in situ* by adding equimolar amounts of various catecholate dianions in acetonitrile solution: [Fe(**L2**)(DBC)]$^+$ (**a**), [Fe(**L2**)(3-MCAT)]$^+$ (**b**), [Fe(**L2**)(CAT)]$^+$ (**c**), [Fe(**L2**)(TCC)]$^+$ (**d**).

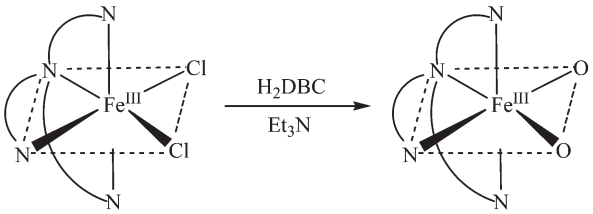

Scheme 3 Schematic illustration of coordination of DBC^{2-} to the iron(III) centre.

Table 4 Electronic spectral data (λ_{max} in nm, ε_{max} in M^{-1} cm^{-1} in parenthesis) for iron(III) complexes[a] and their catecholate[b] adducts in acetonitrile solution

Added catecholate	[Fe(**L1**)Cl_2]Cl	[Fe(**L2**)Cl_2]Cl	[Fe(**L3**)Cl_2]Cl	[Fe(**L4**)Cl_2]Cl	[Fe(**L5**)Cl_2]Cl	[Fe(**L6**)Cl_2]Cl
None[a]	348 (3700)	359 (2850)	350 (4735)	362 (4500)	365 (3865)	369 (4380)
	317 (7150)	304 (2940)	290 (6305)	304 (7640)	304 (4855)	296 (4770)
	250 (13 880)	250 (8040)	253 (11 050)	250 (14 835)	240 (7840)	250 (9740)
DBC^{2-} [b]	870 (2045)	880 (2320)	910 (2305)	855 (1990)	780 (2250)	920 (2480)
	530 (1780)	534 (1665)	570 (3165)	527 (1890)	502 (2470)	563 (3025)
3-$MCAT^{2-}$ [b]	804 (1835)	828 (2035)	875 (1790)	814 (1800)	755 (1515)	866 (1830)
	518 (1620)	530 (1650)	545 (2810)	491 (1885)	500 (1600)	512 (2685)
CAT^{2-} [b]	778 (1845)	788 (2020)	810 (1690)	774 (1815)	735 (1655)	818 (1745)
	508 (1655)	478 (1660)	508 (2490)	478 (1930)	480 (1740)	490 (2290)
TCC^{2-} [b]	685 (1915)	700 (2105)	750 (sh)	710 (sh)	720 (sh)	765 (sh)
	520 (2065)	493 (1880)	521 (2555)	505 (2610)	522 (2500)	517 (2675)

[a] Concentration of the iron(III) complexes, 4×10^{-4} M. The ratio of the added ligand to iron(III) complexes was 1 : 1; the anions were generated by adding 2 equiv. of triethylamine. [b] DBC^{2-} = 3,5-di-*tert*-butylcatechol; 3-$MCAT^{2-}$ = 3-methylcatechol; CAT^{2-} = catechol; TCC^{2-} = 3,4,5,6-tetrachlorocatechol.

center in the catecholate adducts is modified upon changing the primary ligand environment. Also, the position of the low energy catecholate-to-Fe(III) LMCT band in the complex–substrate adducts $[Fe(L)(catecholate)]^+$ generated from $[Fe(L)Cl_2]^+$ and two equivalents of Et_3N is found to be shifted to higher energies as the substituents[20–34] on the catecholate ring are varied from electron-releasing to electron-withdrawing as observed[20,25,34,46] previously: DBC^{2-} > 3Me-CAT^{2-} > CAT^{2-} > TCC^{2-} (Table 4). This is expected as the electron-releasing substituents on the catecholate ring would decrease the energy of the low energy band while the electron-withdrawing substituents enhance it,[20–34,46] thus reflecting the importance of electronic effects expressed by the substituents on catechols.

When **1a** is treated with one equivalent of H_2DBC no spectral change is observed. On the addition of one equivalent of Et_3N no spectral change is observed, revealing that the added base is used to abstract the proton from the $-^+N(H)Me_2$ moiety rather than H_2DBC. On adding a second equivalent of Et_3N to the reaction mixture two characteristic catecholate-to-iron(III) LMCT bands are observed illustrating that the deprotonation of H_2DBC is followed by catecholate adduct formation. Addition of a third equivalent of Et_3N leads to an increase in intensities of the LMCT bands and the spectra obtained are in good agreement with that for $[Fe(\mathbf{L1})(DBC)]^+$. The addition of a fourth equivalent of Et_3N fails to effect any significant change in the spectral bands. All these observations reveal that three equivalents of Et_3N are required to effect the coordination of the $-NMe_2$ group as well as the DBC^{2-} dianion to the iron(III) centre bound to all the four nitrogens of the 4N ligand.

Electrochemical behavior

The redox behaviour of the iron(III) complexes and their catecholate adducts generated *in situ* in acetonitrile solution was studied on a stationary platinum sphere electrode by employing cyclic (CV) and differential pulse voltammetry (DPV). For **1–6**, a cathodic (−0.052–−0.225 V) as well as an anodic wave (0.094–−0.035 V, Fig. 4) are observed. The $E_{1/2}$ values of the

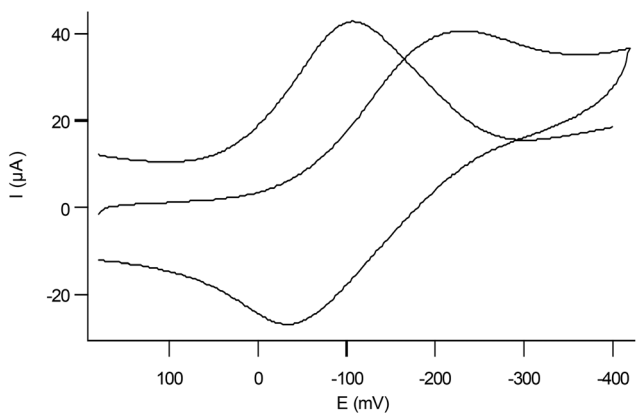

Fig. 4 Cyclic (CV) and differential pulse voltammogram (DPV) of **5** in acetonitrile solution at 25 °C. Supporting electrolyte: 0.1 M TBAP. Scan rate: for CV 50 mV s^{-1}, for DPV 5 mV s^{-1}.

Table 5 Electrochemical data for $[Fe(L)Cl_2]^+$ [a] and $[Fe(L)(DBC)]^+$ [b] in acetonitrile at 25.0 ± 0.2 °C at a scan rate of 50 mV s^{-1} (CV) and 5 mV s^{-1} (DPV)

			$E_{1/2}$ (V)		
Complexes	E_{pc}/V	E_{pa}/V	CV	DPV	Redox process
$[Fe(\mathbf{L1})Cl_2]Cl$	−0.064	0.036	−0.014	0.022	$Fe^{III} \rightarrow Fe^{II}$
$[Fe(\mathbf{L1})Cl_2]Cl + H_2DBC$	−0.072	0.045	0.013	0.008	$Fe^{III} \rightarrow Fe^{II}$
$[Fe(\mathbf{L1})(DBC)]^+$				0.345	$DBSQ \rightarrow DBC$
				−0.010	$Fe^{III} \rightarrow Fe^{II}$
$[Fe(\mathbf{L2})Cl_2]Cl$	−0.125	−0.014	−0.069	−0.037	$Fe^{III} \rightarrow Fe^{II}$
$[Fe(\mathbf{L2})Cl_2]Cl + H_2DBC$	−0.120	−0.012	−0.066	−0.043	$Fe^{III} \rightarrow Fe^{II}$
$[Fe(\mathbf{L2})(DBC)]^+$				0.290	$DBSQ \rightarrow DBC$
				−0.048	$Fe^{III} \rightarrow Fe^{II}$
$[Fe(\mathbf{L3})Cl_2]Cl$	−0.052	0.094	0.021	0.047	$Fe^{III} \rightarrow Fe^{II}$
$[Fe(\mathbf{L3})Cl_2]Cl + H_2DBC$	−0.045	0.091	0.023	0.018	$Fe^{III} \rightarrow Fe^{II}$
$[Fe(\mathbf{L3})(DBC)]^+$				0.368	$DBSQ \rightarrow DBC$
				0.034	$Fe^{III} \rightarrow Fe^{II}$
$[Fe(\mathbf{L4})Cl_2]Cl$	−0.081	0.032	−0.024	−0.007	$Fe^{III} \rightarrow Fe^{II}$
$[Fe(\mathbf{L4})Cl_2]Cl + H_2DBC$	−0.076	0.029	−0.023	−0.003	$Fe^{III} \rightarrow Fe^{II}$
$[Fe(\mathbf{L4})(DBC)]^+$				0.312	$DBSQ \rightarrow DBC$
				−0.023	$Fe^{III} \rightarrow Fe^{II}$
$[Fe(\mathbf{L5})Cl_2]Cl$	−0.225	−0.035	−0.130	−0.105	$Fe^{III} \rightarrow Fe^{II}$
$[Fe(\mathbf{L5})Cl_2]Cl + H_2DBC$	−0.221	−0.036	−0.128	−0.110	$Fe^{III} \rightarrow Fe^{II}$
$[Fe(\mathbf{L5})(DBC)]^+$				0.195	$DBSQ \rightarrow DBC$
				−0.132	$Fe^{III} \rightarrow Fe^{II}$
$[Fe(\mathbf{L6})Cl_2]Cl$	−0.104	0.018	−0.043	−0.028	$Fe^{III} \rightarrow Fe^{II}$
$[Fe(\mathbf{L6})Cl_2]Cl + H_2DBC$	−0.098	0.012	−0.043	−0.032	$Fe^{III} \rightarrow Fe^{II}$
$[Fe(\mathbf{L6})(DBC)]^+$				0.324	$DBSQ \rightarrow DBC$
				−0.043	$Fe^{III} \rightarrow Fe^{II}$

[a] Potential measured *vs.* $Ag(s)/Ag^+$ (0.01 M, 0.10 M TBAP); add 0.544 V to convert to NHE. [b] Generated by adding one equivalent of H_2DBC and two equivalents of triethylamine to complex $[Fe(L)Cl_2]^+$.

Fe^{III}/Fe^{II} redox couple of the complexes (DPV, Table 5) vary in the order, $[Fe(\mathbf{L1})Cl_2]^+$ > $[Fe(\mathbf{L2})Cl_2]^+$ < $[Fe(\mathbf{L3})Cl_2]^+$ > $[Fe(\mathbf{L4})Cl_2]^+$ > $[Fe(\mathbf{L5})Cl_2]^+$ < $[Fe(\mathbf{L6})Cl_2]^+$ revealing that the Lewis acidity of the iron(III) centre is determined by the donor functionalities of the primary ligand. Thus upon replacing the $-NMe_2$ group in **1** by the $-NEt_2$ group to give **2**, the redox potential is shifted to a negative value. The weaker coordination of the sterically hindered nitrogen of the $-NEt_2$ group is expected to increase the positive charge on iron(III) and raise the Fe^{III}/Fe^{II} redox potential; however the chloride ions become coordinated more strongly and decrease the Lewis acidity of the iron(III) centre.[34,41,44–46] Upon replacing both the pyridyl moieties in **1** by 6-methylpyridyl moieties to give **3**, the redox potential is shifted to a more positive value, which is on account of the weaker coordination of the sterically hindering 6-methylpyridyl moiety making the iron(III) centre more Lewis acidic. However, replacing one of the pyridyl moieties in **1** by an imidazolyl moiety to obtain **4** the redox potential is shifted to a negative value as the stronger coordination of the imidazolyl nitrogen atom makes the iron(III) centre less Lewis acidic. The same trend is observed for **5** also, upon replacing both the pyridylmethyl arms in **1** by imidazolylmethyl arms as in **5** the redox potential is shifted to a negative value by rendering the iron(III) centre less Lewis acidic (*cf.* above). Also, upon replacing both the pyridyl moieties in **1** by quinolyl moieties to

give **6** the redox potential is shifted to a slightly negative value due to the weaker coordination of the bulky quinolyl moiety, as expected. Upon adding one equivalent of H_2DBC to **1–6** in acetonitrile solution, the DBSQ/H_2DBC redox wave is overlaid on the Fe^{III}/Fe^{II} redox wave (0.018–0.110 V). When 2 equivalents of Et_3N are added, the Fe^{III}/Fe^{II} redox potential is slightly shifted to a more negative value due to bidentate coordination of DBC^{2-} and the new redox wave in the more positive potential range corresponds to the DBSQ/DBC^{2-} redox couple.[44–46]

Catechol dioxygenase activity of iron(III) complexes

When an acetonitrile solution of the DBC^{2-} adducts $[Fe(L)(DBC)]^+$ generated *in situ* by reacting **1–6** with H_2DBC pretreated with two equivalents of Et_3N was exposed to dioxygen, the intensities of both the DBC^{2-}-to-iron(III) LMCT bands (850–920, 500–570 nm) decrease with time (Fig. 5, Table 6). All the adducts were found to react with molecular oxygen and the oxygenation reactions follow a pseudo-first order kinetics due to the excess of dioxygen used, as judged from the linearity of the plot of [1 + log(absorbance)] *vs.* time (Fig. 6). The second order rate constants (= $k_{obs}/[O_2]$, Table 6) of the reactions were then calculated.[25,41,44–46] The products of cleavage of H_2DBC in acetonitrile solvent (Table 6) were identified (**7–14**, Scheme 4) using GC-MS and ^{1}H NMR techniques and quantified by GC analysis. Interestingly, the adducts $[Fe(L)(DBC)]^+$ of **1–6** were reacted with dioxygen over 24 h to afford extradiol (8–55%) and intradiol cleavage products (23–74%, Table 6) along with very small amounts of other products. The extradiol cleavage leads to two regio-isomeric products,[36–38,44] namely 4,6-di-*tert*-butyloxepine-2,3-dione (**7**) and 5,7-di-*tert*-butyloxepine-2,3-dione (**9**), which are obtained by insertion of an oxygen atom into H_2DBC and two more regio-isomeric products namely 3,5-di-*tert*-butyl-2-pyrones (**8**) and 4,6-di-*tert*-butyl-2-pyrones (**10**) have been obtained from **7** and **9** respectively by the loss of CO.[36–39,44] The intradiol cleavage results in two products, namely 3,5-di-*tert*-butyl-1-oxacyclohepta-3,5-diene-2,7-dione (**11**) and 3,5-di-*tert*-butyl-5-(carboxymethyl)-2-furanone (**12**) and the side products are 3-*tert*-butylfuran-2,5-dione (**13**) and 3,5-di-*tert*-butyl-1,2-benzoquinone (**14**). Interest-

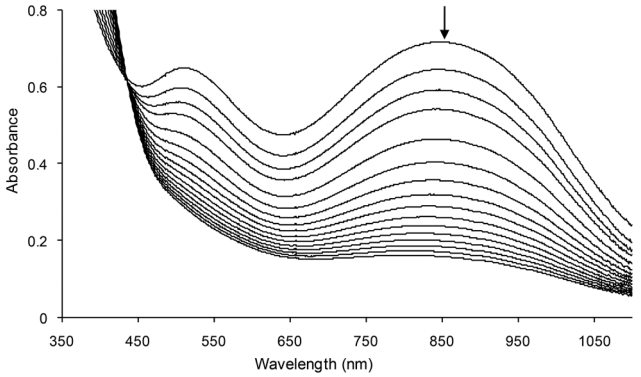

Fig. 5 Progress of the reaction of adduct $[Fe(L4)(DBC)]^+$ with O_2 in ACN solution. The disappearance of the DBC^{2-}-to-iron(III) charge transfer band is monitored.

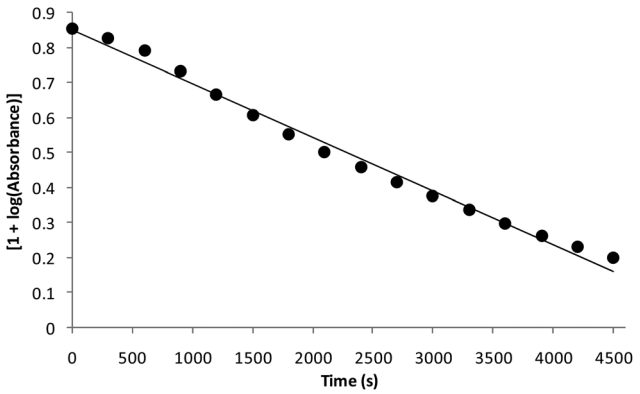

Fig. 6 Plots of [1 + log(absorbance)] *vs.* time for the reaction of $[Fe(L4)(DBC)]^+$ (4×10^{-4} M) with O_2 at 25 °C in acetonitrile solution.

Table 6 Kinetic data[a] for oxidative cleavage of H_2DBC catalyzed by iron(III) complexes in acetonitrile

	Cleavage products in %				
Complex	Extradiol	Intradiol	Others	*E*/*I* ratio	K ($\times 10^{-2}$ M^{-1} s^{-1})
$[Fe(L1)Cl_2]Cl$	4.2 (**7**), 20.6 (**8**) 6.4 (**9**), 23.8 (**10**)	34.0 (**11**, **12**)	5.2 (**13**, **14**)	1.6	1.12 ± 0.02
$[Fe(L2)Cl_2]Cl$	3.7 (**7**), 15.6 (**8**) 5.2 (**9**), 17.5 (**10**)	28.1(**11**, **12**)	4.1 (**13**, **14**)	1.5	0.87 ± 0.04
$[Fe(L3)Cl_2]Cl$	19.9 (**8**) 5.6 (**9**) 19.5 (**10**)	30.0 (**11**, **12**)	3.4 (**13**, **14**)	1.5	1.20 ± 0.03
$[Fe(L4)Cl_2]Cl$	10.2 (**8**) 2.3 (**9**), 12.1 (**10**)	48.0 (**11**, **12**)	8.0 (**13**, **14**)	0.5	2.47 ± 0.03
$[Fe(L5)Cl_2]Cl$	2.1 (**8**) 5.7 (**10**)	74.2 (**11**, **12**)	4.0 (**13**, **14**)	0.1	4.83 ± 0.01
$[Fe(L6)Cl_2]Cl$	2.8 (**7**), 16.5 (**8**) 4.4 (**9**), 24.3 (**10**)	23.6 (**11**, **12**)	5.3 (**13**, **14**)	2.0	1.34 ± 0.04

[a] $k_{O_2} = k_{obs}/[O_2]$. The solubility of O_2 in acetonitrile is accepted to be 8.1 mM at 25 °C. The kinetic data were obtained by monitoring the disappearance of the lower-energy DBC^{2-}-to-iron(III) LMCT band.

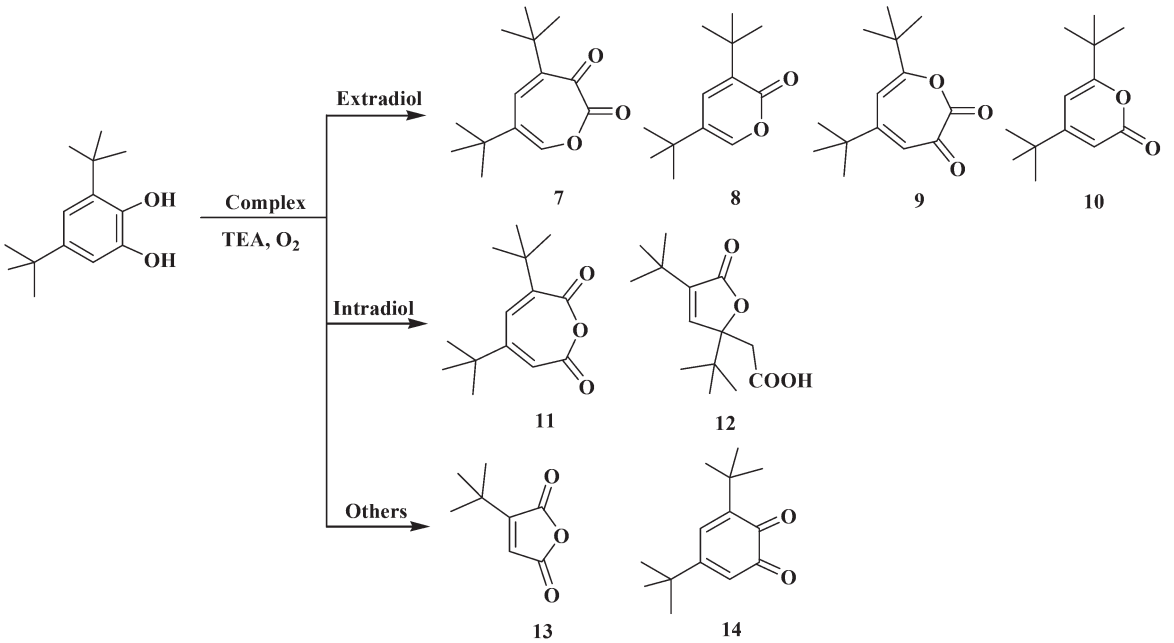

Scheme 4 Products of catechol cleavage of H_2DBC mediated by $[Fe(L)Cl_2]^+$ complexes using molecular oxygen: 4,6-di-*tert*-butyloxepine-2,3-dione (**7**), 3,5-di-*tert*-butyl-2-pyrone (**8**), 5,7-di-*tert*-butyloxepine-2,3-dione (**9**), 4,6-di-*tert*-butyl-2-pyrone (**10**), 3,5-di-*tert*-butyl-1-oxacyclohepta-3,5-diene-2,7-dione (**11**), 3,5-di-*tert*-butyl-5-(carboxymethyl)-2-furanone (**12**), 3-*tert*-butylfuran-2,5-dione (**13**), 3,5-di-*tert*-butyl-1,2-benzoquinone (**14**).

ingly, the trend in the *E*/*I* ratio follows the order **1** (1.6) ≥ **2** (1.5) ≈ **3** (1.5) > **4** (0.5) > **5** (0.1) < **6** (2.0), which reveals that the stereoelectronic properties of 4N ligand donor functionalities dictate the regiospecificity of catechol cleavage.

Most of the iron(III) complexes of 3N ligands yield a major amount of extradiol products along with intradiol cleavage products[35–42,44] due to the presence of a vacant coordination site in the catechol adduct for dioxygen binding. In contrast, several iron(III) complexes of tetradentate tripodal or linear 4N ligands have been reported to cleave catechol to intradiol cleavage products either exclusively or with small amounts of extradiol cleavage products.[20–23,25–27,30,32,36,43] Interestingly, the adduct $[Fe(\mathbf{L1})(DBC)]^+$ with no vacant coordination site for oxygen binding affords higher amounts of extradiol (55%) and lower amounts of intradiol (34%) cleavage products (*E*/*I*, 1.6). Also, the amount of extradiol cleavage products obtained for **1** is higher than those for the previously reported iron(III) complexes of 4N ligands.[20,22,27,43] Thus the adduct[20] $[Fe(TPA)(DBC)]^+$ reacts with dioxygen to yield 98% of intradiol cleavage products; however, when one of the pyridylmethyl arms in the adduct is replaced by the $-CH_2-NMe_2$ arm to give $[Fe(\mathbf{L1})(DBC)]^+$, the extradiol cleavage product is obtained, illustrating that the $-NMe_2$ donor plays a vital role in dictating the cleavage pathway. However, the yield of the extradiol product is lower than that for the adduct[46] $[Fe(L)(DBC)]^+$, where L is a linear 4N ligand with the diazapane backbone, which favours bidentate coordination of monoanionic catecholate. This observation has been illustrated by invoking the involvement of both dioxygen and substrate activation mechanisms (Scheme 5).[22–27,36–46] The iron(II)-DBSQ species formed undergoes either substrate activation or dioxygen activation.[5,17,24,38] In the substrate activation pathway, in the absence of a vacant site, dioxygen attacks the catechol carbon in the iron(II)-DBSQ intermediate to form the cyclohexadienyl peroxide intermediate (Scheme 5) which undergoes acyl migration to yield intradiol products.[22–27,36–46] On the other hand, oxygen activation involves attack of dioxygen on the vacant site created by the displacement of the coordinated $-NMe_2$ group in iron(II)-DBSQ species to form the same cyclohexadienyl peroxide intermediate (Scheme 5). Acyl migration in the intermediate gives intradiol cleavage products[36–46] while alkenyl migration yields extradiol cleavage products.[5,17,24,38,44] The latter involves cleavage of the O–O bond in the intermediate, followed by insertion of one oxygen atom into the aromatic ring to form a lactone intermediate, which proceeds to form the observed pyrone by loss of CO.

In $[Fe(\mathbf{L1})(DBC)]^+$, the coordinated $-NMe_2$ rather than the pyridyl nitrogen donor in the adduct ($Fe-N4_{amine}$, 2.35; $Fe-N1_{py}$, 2.35 Å; *cf.* above) is preferably detached from the coordination sphere during the formation of the cyclohexadienyl peroxide intermediate. Furthermore, spectrophotometric titration of $[Fe(\mathbf{L1})Cl_2]^+$ and H_2DBC requires two equivalents of triethylamine for obtaining the maximum absorption intensity for the catecholate-to-iron(III) LMCT band, indicating that the $-NMe_2$ group does not act as an internal base and that both the detachment of the $-NMe_2$ group and binding of dioxygen on the iron(II) centre in the iron(II)-DBSQ species occur simultaneously (Scheme 5). So, it is clear that a vacant or solvent-coordinated site in the catecholate adducts is essential to form the cyclohexadienyl peroxide species. An analysis of computed geometry of the catecholate adduct (Fig. 2)

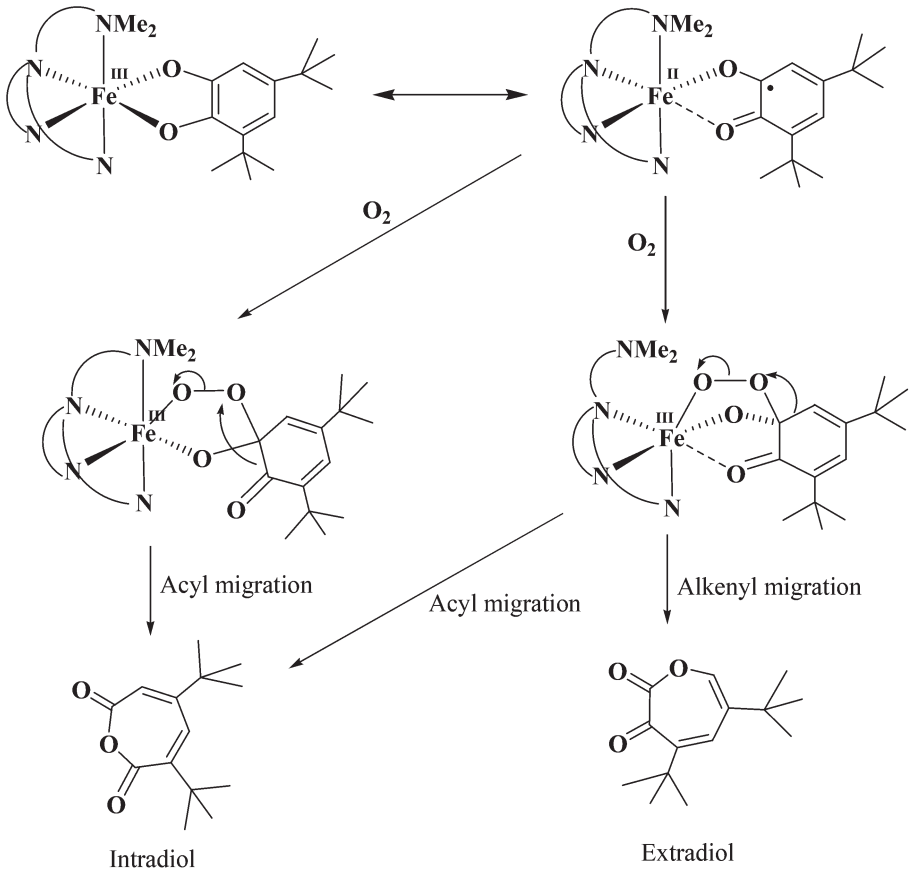

Scheme 5 Proposed oxidative cleavage mechanism for DBC^{2-} of **1–6**.

reveals that the $Fe–O_{catecholate}$ bonds (2.01, 2.08 Å) are asymmetric, which would favour more the dissociation of the Fe–O1 bond (C═O1, 1.29, C–O2, 1.31 Å) and hence alkenyl migration to achieve extradiol cleavage more than the intradiol cleavage product. Upon replacing the $–NMe_2$ group in $[Fe(\mathbf{L1})(DBC)]^+$ by the $–NEt_2$ group to give $[Fe(\mathbf{L2})(DBC)]^+$, 42% of extradiol cleavage products and 28% of intradiol cleavage products (*E*/*I*, 1.5) are obtained. The detachment of the $–NEt_2$ group is encouraged by its bulkiness, which is higher than that of the $–NMe_2$ group, during oxygen binding and thereby enhances the cleavage product yield. However, the yields of both extradiol and intradiol cleavage products decrease, revealing that the steric bulk of the $–NEt_2$ group does not favor O_2 attack.

Interestingly, upon replacing both the pyridyl moieties in $[Fe(\mathbf{L1})(DBC)]^+$ by imidazolyl moieties to give $[Fe(\mathbf{L5})(DBC)]^+$, the intradiol cleavage product is obtained in higher yields (*E*, 8%; *I*, 74%; *E*/*I*, 0.1). The drastic decrease in regiospecificity is obviously on account of stronger coordination of the imidazolyl arm making the $Fe–O_{catecholate}$ bonds less asymmetric (Fe–O1, 204; Fe–O2, 2.02 Å), disfavouring alkenyl migration and hence intradiol cleavage. It may be noted that the stronger coordination of the imidazolyl nitrogen donor slightly weakens the $Fe–NMe_2$ bond ($Fe–N_{amine}$, 2.37 Å, *cf.* above), however the extradiol yield is decreased. As expected, the replacement of one of the pyridyl donors in $[Fe(\mathbf{L1})(DBC)]^+$ by an imidazolyl nitrogen donor to give $[Fe(\mathbf{L4})(DBC)]^+$, a decreased regiospecificity (*E*, 25%; *I*, 48%; *E*/*I*, 0.5) is observed. In contrast, upon replacing both the pyridyl donors in $[Fe(\mathbf{L1})(DBC)]^+$ by quinolyl donors to give $[Fe(\mathbf{L6})(DBC)]^+$, the regiospecificity increases (*E*, 48%; *I*, 24%; *E*/*I*, 2.0). Obviously, it is the large asymmetry in binding of the DBC^{2-} (Fe–O1, 2.11; Fe–O2, 2.02 Å) which favours alkenyl migration further and hence enhances the extradiol cleavage yield. Interestingly, a plot of *E*/*I* against the difference in the $Fe–O_{catecholate}$ bond lengths is linear (Fig. 7). The bulkiness of the quinolyl moiety accounts for the decrease in both the total and extradiol yield, lower than that for $[Fe(\mathbf{L1})(DBC)]^+$, by discouraging the dioxygen attack. Similarly, the replacement of both the pyridyl arms in $[Fe(\mathbf{L1})(DBC)]^+$ by 6-methylpyridyl arms to give $[Fe(\mathbf{L3})(DBC)]^+$, the steric effect of methyl groups on the pyridyl ring leads to lower yields of cleavage products, but does not affect the regiospecificity (*E*, 45%; *I*, 30%; *E*/*I*, 1.5), as expected. Thus, the pyridyl(**1**, **2**)/6-methylpyridyl(**3**)/quinolyl(**6**) nitrogen donors facilitate alkenyl migration leading to high extradiol cleavage products while the imidazolyl nitrogen donor(s) (**4**, **5**) favor(s) acyl migration leading to higher intradiol cleavage products. The decrease in the Lewis acidity of the iron(III) centre due to coordination of a strong donor like imidazole does not facilitate dioxygen attack leading to a decreased extradiol cleavage product. So, the ligand donor functionalities strongly influ-

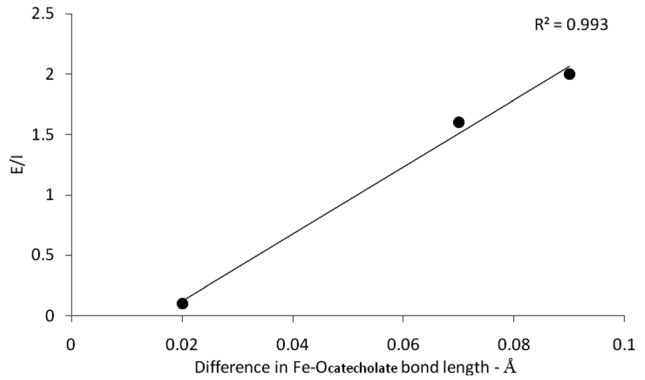

Fig. 7 Plots of *E*/*I* *vs.* difference in the Fe–$O_{catecholate}$ bond length (Å).

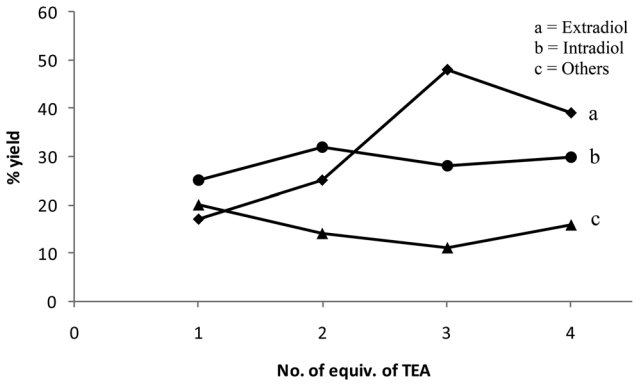

Fig. 8 Variation of the product yield with no. of equivalents of TEA in the oxidative cleavage of H_2DBC by **1a**.

ence the extradiol to intradiol product selectivity (*E*/*I*, 0.1–2.0) by controlling the symmetry of the Fe–$O_{catecholate}$ bonds. Also, interestingly, we have observed a correlation between the ligand donor functionalities and the regio-isomer selectivity in the extradiol cleavage (Fig. S2†), which can be illustrated using the two pathways in Scheme S1.†

To study the effect of coordinated terminal alkyl amine nitrogen on the catechol cleavage pathway, **1** was treated with an equimolar amount of dil. HCl to obtain **1a** in which the amine nitrogen of the terminal –NMe_2 group rather than the pyridyl nitrogen is protonated (*cf.* above) and then detached from the coordination sphere. When **1a** is treated with one equivalent of H_2DBC and one equivalent of Et_3N and then exposed to dioxygen, 12% of extradiol and 15% of intradiol cleavage products (*E*/*I*, 0.8) are observed (Table 7). When two equivalents of Et_3N are used, a higher amount of cleavage products (*E*, 25%; *I*, 32%; *E*/*I*, 0.8) is observed. Interestingly, when three equivalents of triethylamine are added a higher amount of extradiol cleavage products (*E*, 48%; *E*/*I*, 1.7) is observed with the product distribution being almost the same as that observed for $[Fe(\mathbf{L1})(DBC)]^+$ (*cf.* above). So it is clear that creation of a vacant site on the semiquinone intermediate by detachment of the coordinated –NMe_2 group in the adduct $[Fe(\mathbf{L1})(DBC)]^+$ for molecular oxygen attack is vital to achieve extradiol cleavage products (Fig. 8). Hence the addition of a fourth equivalent of Et_3N leads to a lower amount of extradiol cleavage products (*E*, 39; *I*, 30%; *E*/*I*, 1.3). All these observations reveal that both ligand electronic and steric factors of the ligand donor functionalities play a vital role in dictating the cleavage pathway.

Table 7 Effect of the added Et_3N base on oxidative cleavage products of H_2DBC mediated by $[Fe(HL1)Cl_3]Cl$ **1a** using molecular oxygen

Equivalents of Et_3N	Extradiol	Intradiol	Quinone + others	*E*/*I*
1	12.0	15.0	10.0	0.80
2	25.0	32.0	12.0	0.78
3	48.0	28.0	07.0	1.71
4	39.0	30.0	16.0	1.30

Conclusions

Iron(III) complexes of a few systematically varied tripodal tetradentate 4N ligands containing a sterically hindering –NMe_2 alkylamine arm have been isolated and characterized by ESI-MS, electronic spectral and electrochemical techniques. The complex cation of **1a** shows a distorted octahedral iron(III) coordination geometry with the ligand facially coordinated to iron(III) and the protonated amine nitrogen atom of the 4N ligand remaining not coordinated. The iron(III) complexes interact with the substrate 3,5-di-*tert*-butylcatechol (H_2DBC) in the presence of two equivalents of Et_3N as a base to form the adducts of the type $[Fe(L)(DBC)]^+$, as revealed by the observation of two catecholate-to-iron(III) LMCT bands in the visible region. Remarkably, these adducts afford extradiol (8–55%) and intradiol (74–23%) cleavage products and the amount of extradiol cleavage products obtained depends strongly on the ligand architecture. The ability of one of the parent complexes to cleave H_2DBC has been studied as a function of the amount of base added to deprotonate the substrate and this study reveals that displacement of the weakly coordinated –NMe_2 group in the substrate-bound complex facilitates dioxygen attack. The decrease in the Lewis acidity of the iron(III) centre due to coordination of a strong donor like imidazole does not facilitate dioxygen attack leading to a decreased extradiol cleavage product. The extradiol to intradiol product selectivity (*E*/*I*, 0.1–2.0) depends upon the asymmetry in bidentate coordination of catecholate, as determined by the stereoelectronic properties of the ligand donor functionalities.

Acknowledgements

We sincerely thank the Department of Science and Technology, New Delhi, for Research Associateship under DST Nano Mission Project [Scheme no. SR/NM/NS-110/2010(G)] and the Department of Science & Technology, SERB, for the award of Fast track Young Scientist to P. V. (no. SB/FT/CS-071/2012). We also thank the Director, National Institute for Interdisciplinary Science and Technology (NIIST)-CSIR, Trivandrum for provid-

ing the computational facility and Dr C. H. Suresh, CSIR-NIIST, Trivandrum for fruitful discussions. This work was also supported by Indo-French Centre (IFCPAR) [Scheme no. IFC/A/4109-1/2009/993]. We thank the Department of Science and Technology (FIST program), New Delhi for the use of the diffractometer in School of Chemistry.

References

1 J. D. Lipscomb and A. M. Orville, in *Degradation Of Environmental Pollutants By Microorganisms and Their Metalloenzymes*, ed. H. Sigel and A. Sigel, Marcel Dekker, New York, 1992, vol. 28, pp. 243–298.
2 A. L. Feig and S. J. Lippard, *Chem. Rev.*, 1994, **94**, 759–805.
3 L. Que Jr. and R. Y. N. Ho, *Chem. Rev.*, 1996, **96**, 2607–2624.
4 E. L. Hegg and L. Que Jr., *Eur. J. Biochem.*, 1997, **250**, 625–629.
5 M. Costas, M. P. Mehn, M. P. Jensen and L. Que Jr., *Chem. Rev.*, 2004, **104**, 939–986.
6 (*a*) E. I. Solomon, T. Burnold, M. I. Davis, J. N. Kemsley, S.-K. Lee, N. Lehnert, F. Neese, A. J. Skulan, Y.-S. Yang and J. Zhou, *Chem. Rev.*, 2000, **100**, 235–350; (*b*) P. C. A. Bruijnincx, G. Von Koten and R. J. M. Klein Gebbink, *Chem. Soc. Rev.*, 2008, **37**, 2716–2744; (*c*) S. Dagley, in *The Bacteria*, ed. J. R. Sokatch and L. N. Ornstron, Academic Press, Orlando, 1986, ch. 10, pp. 527–555; (*d*) A. Levin and M. A. Gealt, in *Biotreatment Of Industrial and Hazardous Waste*, ed. M. A. Levin and M. A. Gealt, Mcgraw-Hill, New York, 1993, pp. 5–7.
7 (*a*) O. Hayaishi, M. Katagiri and S. Rothberg, *J. Am. Chem. Soc.*, 1955, **77**, 5450–5451; (*b*) O. Hayaishi, *Bacteriol. Rev.*, 1966, **30**, 720–731.
8 (*a*) D. H. Ohlenddorf, J. D. Lipscomb and P. C. Weber, *Nature*, 1988, **336**, 403–405; (*b*) D. H. Ohlenddorf, A. M. Orville and J. D. Lipscomb, *J. Mol. Biol.*, 1994, **244**, 586–608; (*c*) M. W. Vetting, C. A. Earhart and D. H. Ohlenddorf, *J. Mol. Biol.*, 1994, **236**, 372–373; (*d*) M. W. Vetting and D. H. Ohlendorf, *Structure*, 2000, **8**, 429–440.
9 (*a*) K. Sugimoto, T. Senda, H. Aoshima, E. Masai, M. Fukuda and Y. Mitsui, *Structure*, 1999, **7**, 953–965; (*b*) N. Sato, Y. Uragami, T. Nishizaki, Y. Takahashi, G. Sazaki, K. Sugimoto, T. Nonaka, E. Masai, M. Fukuda and T. Senda, *J. Mol. Biol.*, 2002, **321**, 621–636.
10 (*a*) S. Han, L. D. Eltis, K. N. Timmis, S. W. Muchmore and J. T. Bolin, *Science*, 1995, **270**, 976–980; (*b*) A. Kita, S. I. Kita, I. Fujisawa, K. Inaka, T. Ishida, K. Horiike, M. Nozaki and K. Miki, *Structure*, 1999, **7**, 25–34.
11 (*a*) L. Que Jr., in *Bioinorganic Catalysis*, ed. J. Reedijk and E. Bouwman, Marcel Dekker Inc., New York, 2nd edn, 1999, pp. 269–321; (*b*) L. Que Jr. and M. F. Reynolds, *Metal Ions Biol. Syst.*, 2000, **37**, 505–525; (*c*) K. D. Koehntop, J. P. Emerson and L. Que Jr., *J. Biol. Inorg. Chem.*, 2005, **10**, 87–93.
12 (*a*) M. I. Davis, E. C. Wasinger, A. Decker, M. Y. M. Pau, F. H. Vaillancourt, J. T. Bolin, L. D. Eltis, B. Hedman, K. O. Hodgson and E. I. Solomon, *J. Am. Chem. Soc.*, 2003, **125**, 11214–11227; (*b*) M. Y. M. Pau, M. I. Davis, A. M. Orville, J. D. Lipscomb and E. I. Solomon, *J. Am. Chem. Soc.*, 2007, **129**, 1944–1958; (*c*) M. Y. M. Pau, J. D. Lipscomb and E. I. Solomon, *Proc. Natl. Acad. Sci. U. S. A.*, 2007, **104**, 18355–18362.
13 (*a*) J. W. Whittaker, J. D. Lipscomb, T. A. Kent, E. Munck, N. R. Orme-Johnson and W. H. Orme-Johnson, *J. Biol. Chem.*, 1984, **259**, 4487–4495; (*b*) A. M. Orville and J. D. Lipscomb, *J. Biol. Chem.*, 1989, **264**, 8791–8801; (*c*) A. E. True, A. M. Orville, L. L. Pearce, J. D. Lipscomb and L. Que Jr., *Biochemistry*, 1990, **29**, 10847–10854.
14 (*a*) A. M. Orville, J. D. Lipscomb and D. H. Ohlendorf, *Biochemistry*, 1997, **36**, 10052–10066; (*b*) A. M. Orville, N. Elango, J. D. Lipscomb and D. H. Ohlendorf, *Biochemistry*, 1997, **36**, 10039–10051.
15 M. Abu-Omar, A. Loaiza and N. Hontzeas, *Chem. Rev.*, 2005, **105**, 2227–2252.
16 (*a*) G. P. Titus, H. A. Mueller, J. Burgner, S. Rodriguez De Cordoba, M. A. Penalva and D. E. Timm, *Nat. Struct. Biol.*, 2000, **7**, 542–546; (*b*) M. I. Davies, A. M. Orville, F. Neese, J. M. Zaleski, J. D. Lipscomb and E. I. Solomon, *J. Am. Chem. Soc.*, 2002, **124**, 602–614; (*c*) M. Xin and T. D. H. Bugg, *J. Am. Chem. Soc.*, 2008, **130**, 10422–10430.
17 (*a*) M. A. Miller and J. D. Lipscomb, *J. Biol. Chem.*, 1996, **271**, 5524–5535; (*b*) E. G. Kovaleva and J. D. Lipscomb, *Science*, 2007, **316**, 453–457; (*c*) E. G. Kovaleva, M. B. Neibergall, S. Chakrabarty and J. D. Lipscomb, *Acc. Chem. Res.*, 2007, **40**, 475–483; (*d*) E. G. Kovaleva and J. D. Lipscomb, *Biochemistry*, 2008, **47**, 11168–11170.
18 (*a*) R. B. Lauffer, R. H. Heistand Ii and L. Que Jr., *J. Am. Chem. Soc.*, 1981, **103**, 3947–3949; (*b*) R. H. Heistand Ii, A. L. Roe and L. Que Jr., *Inorg. Chem.*, 1982, **21**, 676–681; (*c*) R. H. Heistand Ii, R. B. Lauffer, E. Fikrig and L. Que Jr., *J. Am. Chem. Soc.*, 1982, **104**, 2789–2796; (*d*) R. B. Lauffer, R. H. Heistand Ii and L. Que Jr., *Inorg. Chem.*, 1983, **22**, 50–55.
19 (*a*) L. S. White, P. V. Nilsson, L. H. Pignolet and L. Que Jr., *J. Am. Chem. Soc.*, 1984, **106**, 8312–8313; (*b*) L. Que Jr., R. C. Kolanczyk and L. S. White, *J. Am. Chem. Soc.*, 1987, **109**, 5373–5380; (*c*) D. D. Cox and L. Que Jr., *J. Am. Chem. Soc.*, 1988, **110**, 8085–8092; (*d*) D. D. Cox, S. J. Benkovic, L. M. Bloom, F. C. Bradley, M. J. Nelson, L. Que Jr. and D. E. Wallick, *J. Am. Chem. Soc.*, 1988, **110**, 2026–2032.
20 (*a*) H. G. Jang, D. D. Cox and L. Que Jr., *J. Am. Chem. Soc.*, 1991, **113**, 9200–9204; (*b*) Y.-M. Chiou and L. Que Jr., *Inorg. Chem.*, 1995, **34**(14), 3577–3578.
21 (*a*) T. Funabiki, H. Sakamoto, S. Yoshida and K. Tarama, *J. Chem. Soc., Chem. Commun.*, 1979, 754–755; (*b*) T. Funabiki, T. Yamazaki, A. Fukui, T. Tanaka and S. Yoshida, *Angew. Chem., Int. Ed.*, 1998, **37**, 513–515; (*c*) S. Ogo, R. Yamahara, T. Funabiki, H. Masuda and Y. Watanabe, *Chem. Lett.*, 2001, 1062–1063; (*d*) T. Funabiki, A. Fukui, Y. Hitomi, M. Higuchi, T. Yamamoto, T. Tanaka,

F. Tani and Y. Naruta, *J. Inorg. Biochem.*, 2002, **91**, 151–158; (*e*) R. Yamahara, S. Ogo, Y. Watanabe, T. Funabiki, K. Jitsukawa, H. Masuda and H. Einaga, *Inorg. Chim. Acta*, 2000, **300–302**, 587–596; (*f*) T. Funabiki, D. Sugio, N. Inui, M. Maeda and Y. Hitomi, *Chem. Commun.*, 2002, 412–413; (*g*) Y. Hitomi, M. Higuchi, T. Tanaka and T. Funabiki, *Inorg. Chim. Acta*, 2005, **358**, 3465–3470; (*h*) M. Higuchi, Y. Hitomi, H. Minami, T. Tanaka and T. Funabiki, *Inorg. Chem.*, 2005, **44**, 8810–8821; (*i*) R. Yamahara, S. Ogo, H. Masuda and Y. Watanabe, *J. Inorg. Biochem.*, 2002, **88**, 284–294.

22 (*a*) J. H. Lim, H.-J. Lee, K.-B. Lee and H. G. Jang, *Bull. Korean Chem. Soc.*, 1997, **18**, 1166–1172; (*b*) J. H. Lim, T. H. Park, H.-J. Lee, K.-B. Lee and H. G. Jang, *Bull. Korean Chem. Soc.*, 1999, **20**, 1428–1432.

23 (*a*) W. O. Koch and H. J. Krüger, *Angew. Chem., Int. Ed. Engl.*, 1996, **34**, 2671–2674; (*b*) W. O. Koch, V. Schünemann, M. Gerdan, A. X. Trautwein and H. J. Krüger, *Chem. – Eur. J.*, 1998, **4**, 1255–1265.

24 G. Lin, G. Reid and T. D. H. Bugg, *J. Am. Chem. Soc.*, 2001, **123**, 5030–5039; T. D. H. Bugg and G. Lin, *Chem. Commun.*, 2001, 941–952; T. D. H. Bugg, *Tetrahedron*, 2003, **59**, 7075–7101.

25 (*a*) M. Pascaly, M. Duda, F. Schweppe, K. Zurlinden, F. K. Muller and B. Krebs, *J. Chem. Soc., Dalton Trans.*, 2001, 828–837; (*b*) M. Duda, M. Pascaly and B. Krebs, *Chem. Commun.*, 1997, 835–836; (*c*) M. Merkel, D. Schnieders, S. M. Baldeau and B. Krebs, *Eur. J. Inorg. Chem.*, 2004, 783–790; (*d*) M. Merkel, F. K. Müller and B. Krebs, *Inorg. Chim. Acta*, 2002, **337**, 308–316; (*e*) M. Merkel, M. Pascaly, B. Krebs, J. Astner, S. P. Foxon and S. Schindler, *Inorg. Chem.*, 2005, **44**, 7582–7589; (*f*) J.-Y. Xu, J. Astner, O. Walter, F. W. Heinemann, S. Schindler, M. Merkel and B. Krebs, *Eur. J. Inorg. Chem.*, 2006, 1601–1610; (*g*) M. Pascaly, C. Nazikkol, F. Schweppe, A. Wiedemann, K. Zurlinden and B. Krebs, *Z. Anorg. Allg. Chem.*, 2000, **626**, 50–55.

26 P. Mialane, L. Tchertanov, F. Banse, J. Sainton and J. J. Girerd, *Inorg. Chem.*, 2000, **39**, 2440–2444.

27 N. Raffard, R. Carina, A. J. Simaan, J. Sainton, E. Riviere, L. Tchertanov, S. Bourcier, G. Bouchoux, M. Delroisse, F. Banse and J. J. Girerd, *Eur. J. Inorg. Chem.*, 2001, 2249–2254.

28 H. Fujii and Y. Funahasi, *Angew. Chem., Int. Ed.*, 2002, **41**, 3638–3641.

29 (*a*) P. C. A. Bruijnincx, M. Lutz, A. L. Spek, W. R. Hagen, G. Von Koten and R. J. M. Klein Gebbink, *Inorg. Chem.*, 2007, **46**, 8391–8402; (*b*) R. Jastrzebski, B. M. Weckhuysen and P. C. A. Bruijnincx, *Chem. Commun.*, 2013, **49**, 6912–6914.

30 F. Li, M. Wang, P. Li, T. Zhang and L. Sun, *Inorg. Chem.*, 2007, **46**, 9364–9371.

31 M. K. Panda, A. John, M. M. Shaikh and P. Ghosh, *Inorg. Chem.*, 2008, **47**, 11847–11856.

32 A. Panja, S. Goswami, N. Shaikh, P. Roy, M. Manassero, R. J. Butcher and P. Banerjee, *Polyhedron*, 2005, **24**(18), 2921–2932.

33 T. Váradi, J. S. Pap, M. Giorgi, L. Párkányi, T. Csay, G. Speier and J. Kaizer, *Inorg. Chem.*, 2013, **52**(3), 1559–1569.

34 (*a*) R. Viswanathan, M. Palaniandavar, T. Balasubramanian and P. T. Muthiah, *J. Chem. Soc., Dalton Trans.*, 1996, 2519–2525; (*b*) R. Viswanathan and M. Palaniandavar, *J. Chem. Soc., Dalton Trans.*, 1995, 1259–1266; (*c*) R. Viswanathan, M. Palaniandavar, T. Balasubramanian and P. T. Muthiah, *Inorg. Chem.*, 1998, **37**, 2943–2951; (*d*) M. Velusamy, M. Palaniandavar, R. Srinivasagopalan and G. U. Kulkarni, *Inorg. Chem.*, 2003, **42**, 8283–8293; (*e*) M. Velusamy, R. Mayilmurugan and M. Palaniandavar, *Inorg. Chem.*, 2004, **43**, 6284–6293; (*f*) M. Velusamy, R. Mayilmurugan and M. Palaniandavar, *J. Inorg. Biochem.*, 2005, **99**, 1032–1042; (*g*) T. Dhanalakshmi, M. Bhuvaneshwari and M. Palaniandavar, *J. Inorg. Biochem.*, 2006, **100**, 1527–1534; (*h*) M. Palaniandavar, M. Velusamy and R. Mayilmurugan, *J. Chem. Sci.*, 2006, **118**, 601–610; (*i*) M. Palanaiandavar and R. Mayilmurugan, *C. R. Chim.*, 2007, **10**, 366–379; (*j*) R. Mayilmurugan, K. Visvaganesan, E. Suresh and M. Palaniandavar, *Inorg. Chem.*, 2009, **48**, 8771–8783; (*k*) K. Sundaravel, M. Sankaralingam, E. Suresh and M. Palaniandavar, *Dalton Trans.*, 2011, **40**, 8444–8458.

35 (*a*) T. Funabiki, A. Mizoguchi, T. Sugimoto and S. Yoshida, *Chem. Lett.*, 1983, 917–920; (*b*) T. Funabiki, A. Mizoguchi, T. Sugimoto, S. Tada, M. Tsugi, H. Sakamoto and S. Yoshida, *J. Am. Chem. Soc.*, 1986, **108**, 2921–2932.

36 A. Dei, D. Gatteschi and L. Pardi, *Inorg. Chem.*, 1993, **32**, 1389–1395.

37 (*a*) M. Ito and L. Que Jr., *Angew. Chem., Int. Ed. Engl.*, 1997, **36**, 1342–1344; (*b*) D.-H. Jo and L. Que Jr., *Angew. Chem., Int. Ed.*, 2000, **39**, 4284–4287.

38 (*a*) G. Lin, G. Reid and T. D. H. Bugg, *Chem. Commun.*, 2000, 1119–1120; (*b*) G. Lin, G. Reid and T. D. H. Bugg, *J. Am. Chem. Soc.*, 2001, **123**, 5030–5039.

39 T. Oghihara, S. Hikichi, M. Akita and M. Moro-Oka, *Inorg. Chem.*, 1998, **37**, 2614–2615.

40 P. C. A. Bruijnincx, M. Lutz, A. L. Spek, W. R. Hagen, B. M. Weckhuysen, G. Koten and R. J. M. Klein Gebbink, *J. Am. Chem. Soc.*, 2007, **129**, 2275–2286.

41 M. Wagner, C. Limberg and T. Tietz, *Chem. – Eur. J.*, 2009, **15**, 5567–5576.

42 (*a*) S. Paria, P. Halder and T. K. Paine, *Inorg. Chem.*, 2010, **49**(10), 4518–4523; (*b*) P. Halder, S. Paria and T. K. Paine, *Chem. – Eur. J.*, 2012, **18**(37), 11778–11787.

43 D.-H. Jo, Y.-M. Chiou and L. Que Jr., *Inorg. Chem.*, 2001, **40**, 3181–3190.

44 (*a*) K. Visvaganesan, R. Mayilmurugan, E. Suresh and M. Palaniandavar, *Inorg. Chem.*, 2007, **46**, 10294–10306; (*b*) K. Sundaravel, T. Dhanalakshmi, E. Suresh and M. Palaniandavar, *Dalton Trans.*, 2008, 7012–7025; (*c*) T. Dhanalakshmi, E. Suresh and M. Palaniandavar, *Dalton Trans.*, 2009, 8317–8328; (*d*) N. Anitha and M. Palaniandavar, *Dalton Trans.*, 2010, **39**, 1195–1197; (*e*) N. Anitha and M. Palaniandavar, *Dalton Trans.*, 2011,

40, 1888–1901; (*f*) K. Sundaravel, E. Suresh, K. Saminathan and M. Palaniandavar, *Dalton Trans.*, 2011, **40**, 8092–8107.

45 R. Mayilmurugan, E. Suresh and M. Palaniandavar, *Inorg. Chem.*, 2007, **46**, 6038–6049.

46 R. Mayilmurugan, H. Stoeckli-Evans and M. Palaniandavar, *Inorg. Chem.*, 2008, **47**, 6645–6658.

47 (*a*) A. J. Bard and L. R. Faulkner, in *Electrochemical Methods: Fundamentals and Applications*, John Wiley & Sons, New York, 1980, pp. 218; (*b*) D. T. Sawyer, A. Sobkowiak and J. L. Roberts Jr., in *Electrochemistry For Chemists*, Wiley-Interscience, New York, 2nd edn, 1995, pp. 336.

48 G. J. P. Britovsek, J. England and A. J. P. White, *Inorg. Chem.*, 2005, **44**, 8125–8134.

49 M. Balamurugan, R. Mayilmurugan, E. Suresh and M. Palaniandavar, *Dalton Trans.*, 2011, **40**, 9413–9424.

50 *SMART & SAINT Software Reference Manuals Version 5.0*, Bruker Axs Inc., Madison, WI, 1998.

51 G. M. Sheldrick, *SADABS Software for Empirical Absorption Correction*, University Of Göttingen, Germany, 1996.

52 *SHELXTL Reference Manual Version 5.1*, Bruker Axs Inc., Madison, WI, 1998.

53 (*a*) Japan Chemical Society, *Kagaku-Binran Basic Part Ii*, Maruzen, Tokyo, 2nd edn, 1975; (*b*) D. T. Sawyer, *Oxygen Chemistry*, Oxford University Press, New York, 1991.

54 K. R. J. Thomas, M. Velusamy and M. Palaniandavar, *Acta Crystallogr., Sect. C: Cryst. Struct. Commun.*, 1998, **54**, 741–743.

55 M. C. Rodriguez, F. Lambert, I. Morgenstern-Badarau, M. Cesario, J. Guilhem, B. Keita and L. Nadjo, *Inorg. Chem.*, 1997, **36**, 3525–3531.

56 M. J. Frisch, G. W. Trucks, H. B. Schlegel, G. E. Scuseria, M. A. Robb, J. R. Cheeseman, G. Scalmani, V. Barone, B. Mennucci, G. A. Petersson, H. Nakatsuji, M. Caricato, X. Li, H. P. Hratchian, A. F. Izmaylov, J. Bloino, G. Zheng, J. L. Sonnenberg, M. Hada, M. Ehara, K. Toyota, R. Fukuda, J. Hasegawa, M. Ishida, T. Nakajima, Y. Honda, O. Kitao, H. Nakai, T. Vreven, J. A. Montgomery, J. E. Peralta Jr., F. Ogliaro, M. Bearpark, J. J. Heyd, E. Brothers, K. N. Kudin, V. N. Staroverov, R. Kobayashi, J. Normand, K. Raghavachari, A. Rendell, J. C. Burant, S. S. Iyengar, J. Tomasi, M. Cossi, N. Rega, J. M. Millam, M. Klene, J. E. Knox, J. B. Cross, V. Bakken, C. Adamo, J. Jaramillo, R. Gomperts, R. E. Stratmann, O. Yazyev, A. J. Austin, R. Cammi, C. Pomelli, J. W. Ochterski, R. L. Martin, K. Morokuma, V. G. Zakrzewski, G. A. Voth, P. Salvador, J. J. Dannenberg, S. Dapprich, A. D. Daniels, Ö. Farkas, J. B. Foresman, J. V. Ortiz, J. Cioslowski and D. J. Fox, *Gaussian 09, Revision A.1*, Gaussian, Inc., Wallingford, CT, 2009.

